THE STATE OF THE CLIMATE 2020

Ole Humlum

The State of the Climate 2020
Ole Humlum

Report 50, The Global Warming Policy Foundation

About the author

Ole Humlum is former Professor of Physical Geography at the University Centre in Svalbard, Norway, and Emeritus Professor of Physical Geography, University of Oslo, Norway.

Contents

THE STATE OF
THE CLIMATE
2020

Ole Humlum

1.   General overview 2020

This report has its focus on observations, and not the output from numerical models. References and data sources are listed at the end of the report.

Air temperatures

Air temperatures measured near the planet's surface (surface air temperatures) are at the core of many climate deliberations, but the significance of any short-term warming or cooling recorded in these data series should not be overstated. Whenever Earth experiences warm El Niño or cold La Niña episodes, there are major exchanges of heat between the Pacific Ocean and the atmosphere above, eventually showing up as a signal in the global air temperature. However, this does not reflect any change in the total heat content of the ocean–atmosphere system; such heat exchanges are simply a redistribution of energy between the ocean and atmosphere. Evaluating the dynamics of ocean temperatures is therefore just as important as evaluating changes of surface air temperatures.

Considering surface air temperature records since 1850/1880, the year 2020 was very warm – nearly as warm as 2016. In 2019–2020, the decrease in average global temperature characterising 2017 and 2018 was interrupted by a renewed, moderate El Niño episode, underlining the importance of ocean–atmosphere exchanges.

Many Arctic regions experienced record high air temperatures in 2016, but since then, including 2020, conditions have generally been somewhat cooler. The Arctic temperature peak in 2016 may have been affected by heat released from the Pacific Ocean during the strong 2015–16 El Niño, and subsequently transported towards the Arctic region. This underscores how Arctic air temperatures may be affected not only by variations in local conditions but also by variations playing out in geographically remote regions.

Many diagrams in this report focus on the period from 1979 onwards – the satellite era – since when there has been a wide range of observations with nearly global coverage, including temperature. Satellite data provide a detailed view of temperature changes over time at different altitudes in the atmosphere. They reveal that while the widely recognised lower troposphere temperature pause began around 2002, a similar stratospheric temperature plateau had already begun by 1995.

Since 1979, lower troposphere temperatures have increased over both land and oceans, but most clearly over land areas. The most straightforward explanation for this phenomenon is that much of the warming is caused by solar insolation, but there may well be several supplementary reasons, such as changes in cloud cover and land use.

Oceans

The Argo Program, which uses robotic floats to monitor ocean temperatures, has now achieved 15 years of global coverage. During that time it has grown from a relatively sparse array of 1000 floats in 2004 to more than 3900 in January 2021. Since 2004, it has provided a unique ocean temperature data set for depths down to 1900 m. Although the oceans are much deeper than that, and the Argo data series is still relatively short, interesting features are now emerging from these observations.

Since 2004, the upper 1900 m of the oceans have experienced net warming of about 0.07°C. The maximum net warming is about 0.2°C, and affects the uppermost 100 m of the oceans, mainly in regions near the Equator, where solar irradiance is greatest. At greater depths, there has been a small net warming, of about 0.025°C, over the same period. This development in global ocean temperatures is reflected in the equatorial oceans between 30°N and 30°S, which, due to the spherical shape of the planet, represent a huge surface area. Simultaneously, the northern oceans (55–65°N) have on average experienced a marked cooling down to 1400 m depth, and slight warming at greater depths. The southern oceans (55–65°S) on average have seen a slight warming at most depths since 2004, but mainly near the surface. However, averages may be misleading, and quite often better insight is obtained by studying the details, as is discussed later in this report.

Sea level

Global sea levels are monitored by satellite altimetry and by direct measurements from tide gauges along coasts. While the satellite record suggests a global sea-level rise of about 3.3 mm per year, data from tide gauges along coasts all over the world suggest a stable, average sea-level rise of 1–2 mm per year. The measurements do not indicate any recent acceleration (or deceleration) in sea-level rise. The marked difference (a ratio of about 1:2) between the two data sets still has no universally accepted explanation, but it is known that satellite observations face complications in coastal areas (see, e.g. Vignudelli et al. 2019). However, for local coastal planning, it is the tide-gauge data that is relevant, as detailed later in this report.

Sea ice

In 2020, global sea-ice cover extent remained well below the average for the satellite era (since 1979), but a rising trend is now evident. At the end of 2016, global sea-ice extent reached a marked minimum, at least partly caused by the operation of two different natural variation patterns characterising sea ice in the Northern and Southern Hemispheres, respectively. Both variations had simultaneous minima in 2016, with resulting consequences for the global sea-ice extent. The opposite development, towards stable or higher ice extent at both poles, probably began in 2018, and was augmented during 2019 and 2020, especially for Antarctic sea ice. The marked Antarctic 2016 sea-ice reduction was affected by unusual wind conditions.

Snow cover

Variations in global snow-cover extent are driven by changes in the Northern Hemisphere, where most of the major land masses are located. Southern Hemisphere snow-cover extent is essentially controlled by the Antarctic ice sheet, and is therefore relatively stable. Northern Hemisphere average snow cover has also been stable since the advent of satellite observations, although local and regional interannual variations may be large. Considering seasonal changes in the Northern Hemisphere since 1979, autumn extent has been slightly increasing, mid-winter extent has been largely stable, and spring extent has been slightly decreasing. In 2020, Northern Hemisphere seasonal snow cover was somewhat below that of the preceding years.

Storms and hurricanes

The most recent data on numbers of global tropical storms and hurricane accumulated cyclone energy (ACE) are well within the range seen since 1970. In fact, the ACE data series displays a variable pattern over time, with a significant 3.6-year variation, but without any clear trend towards higher or lower values. A longer ACE series for the Atlantic Basin (since 1850), however, suggests a natural cycle of about 60 years' duration for tropical-storm and hurricane ACE. The number of hurricane landfalls in the continental United States remains within the normal range for the entire record since 1851.

2.   The spatial pattern of global surface air temperatures 2020

Global average surface air temperature for 2020 was high, but according to most records slightly cooler than 2016. Each of the years 2016, 2019 and 2020 was affected by El Niño episodes playing out in the Pacific Ocean. In 2017–18, the global surface air temperature was slowly dropping back towards the pre-2015/16 level, but in 2019 this was interrupted by a renewed temperature increase due to a new, moderate El Niño. By the end of 2020, however, a La Niña episode has developed (Figure 22, page 19), and this is likely to push global air temperatures toward a somewhat lower level in 2021.

In 2020, the Northern Hemisphere was characterised by regional temperature contrasts, influenced by the dominant jet stream pattern. The most pronounced development was a long-lasting heatwave in north-west Siberia, clearly visible in Figure 1, and the continuation from 2018/19 of relatively cold conditions in much of North America.

Near the Equator, surface air temperatures were generally near or below the average for the previous ten years. In particular, much of equatorial Pacific Ocean was relatively cold, due to the La Niña episode.

In the Southern Hemisphere, surface air temperatures were near or below the average for the previous ten years. Few land regions were warmer than the average for the last ten years.

In the Arctic (Figure 2), the American and Atlantic sectors were relatively cold, while most of the Russia-Siberian sectors were relatively warm.

The Antarctic was mainly characterised by near-average temperatures in 2020, in continuation of the conditions in 2019.

Summing up, in 2020, global average air temperatures were relatively high, reflecting the 2019–20 moderate El Niño episode playing out in the Pacific Ocean. At the end of 2020, however, this was replaced by a developing La Niña episode. Thus the global surface air temperatures continued to be highly influenced by such oceanographic phenomena.
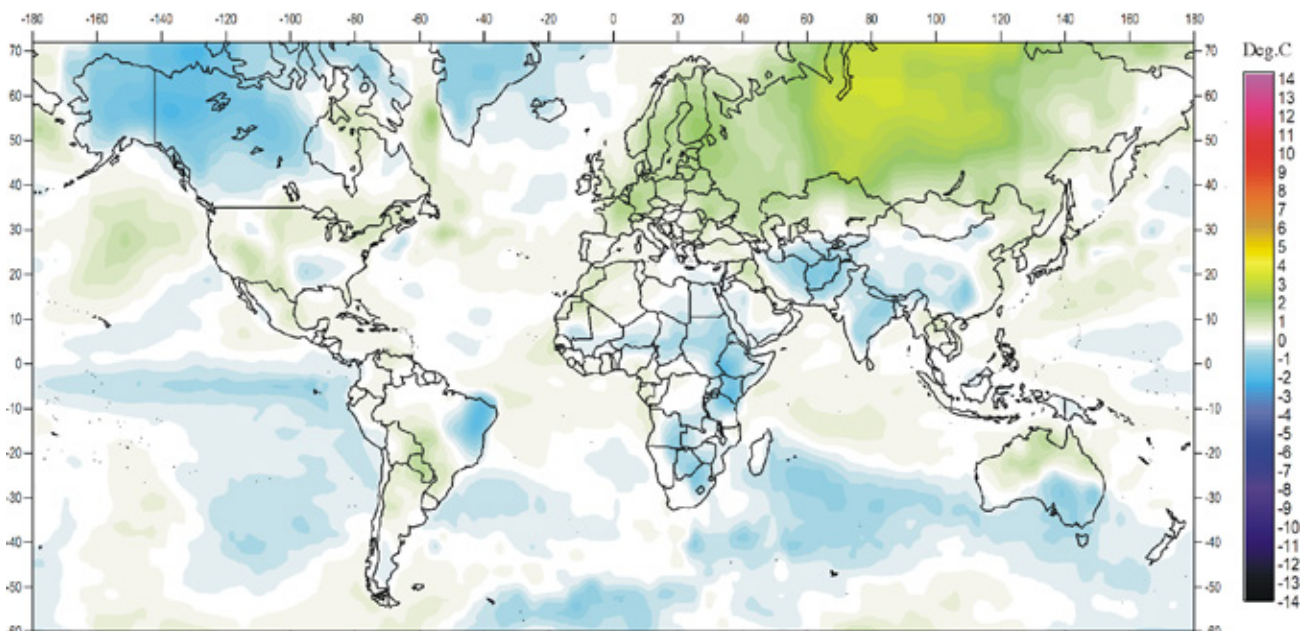
Figure 1: 2020 surface air temperatures compared to the average for the previous 10 years.

Green-yellow-red colours indicate areas with higher temperature than the average, while blue colours indicate lower than average temperatures. Data source: Remote Sensed Surface Temperature Anomaly, AIRS/Aqua L3 Monthly Standard Physical Retrieval 1-degree x 1-degree V006 (https://airs.jpl.nasa.gov/), obtained from the GISS data portal (https://data.giss.nasa.gov/gistemp/maps/index_v4.html).

(a) Arctic　　　　　　　　　　　　　(b) Antarctic
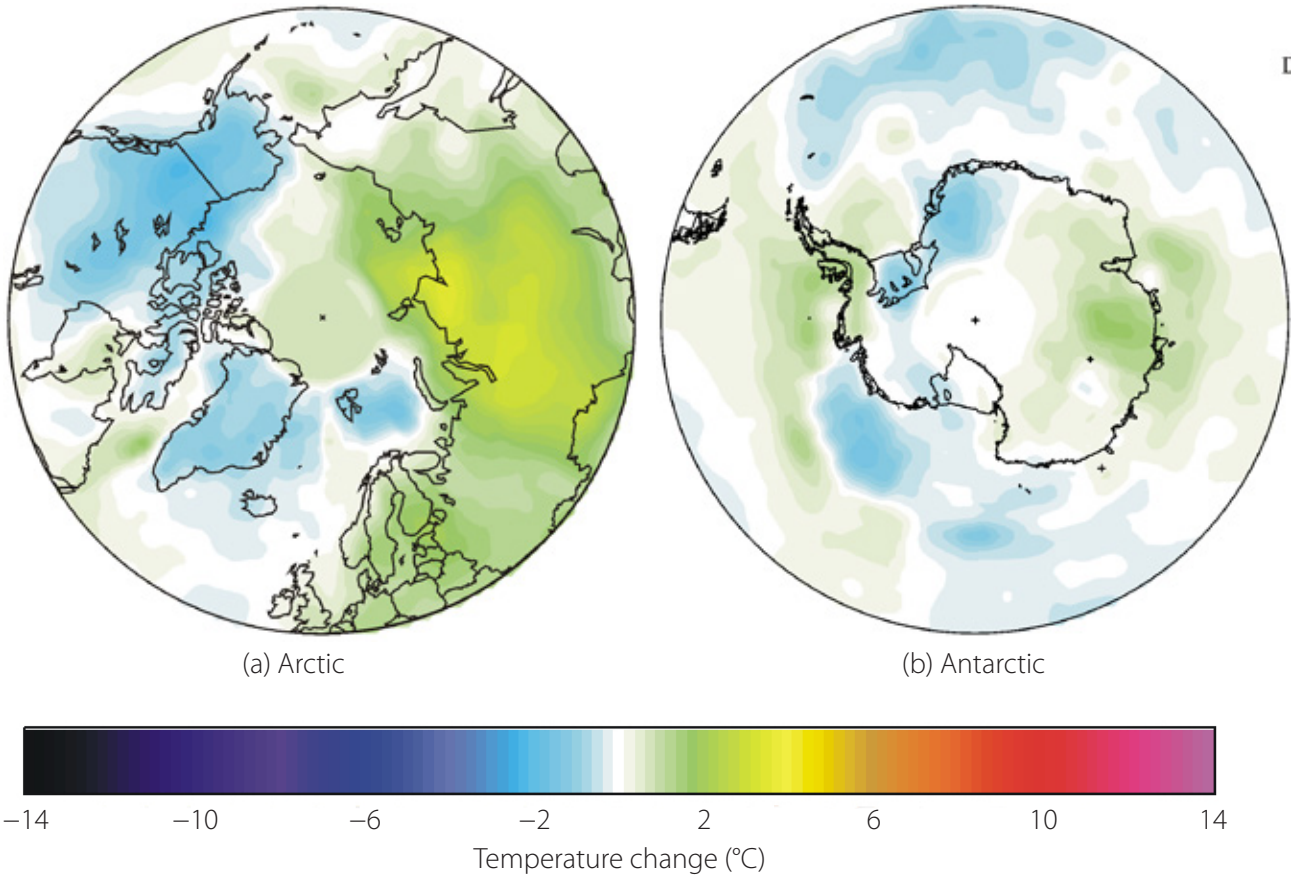
Figure 2: 2020 polar surface air temperatures compared to the average for the previous 10 years.
Green-yellow-red colours indicate areas with higher temperature than the average, while blue colours indicate lower than average temperatures. Data source: Remote Sensed Surface Temperature Anomaly, AIRS/Aqua L3 Monthly Standard Physical Retrieval 1-degree × 1-degree V006 (https://airs.jpl.nasa.gov/), obtained from the GISS data portal (https://data.giss.nasa.gov/gistemp/maps/index_v4.html).

3.   Global monthly lower troposphere temperature since 1979

There are two satellite temperature series for the lower troposphere: from the University of Alabama at Huntsville (UAH) and from Remote Sensing Systems (RSS). Both clearly show a temperature spike associated with the 2015–16 El Niño, a subsequent gradual drop, followed by the onset of a new temperature spike due to the moderate 2019–20 El Niño.

The comparison between the latest (December 2020) record and the May 2015 record (red lines in Figure 3) shows that only a few small adjustments have been made to the UAH series since then, but the RSS series has been subject to large adjustments towards higher temperatures from 2002 onwards; about +0.1°C. This adjustment of the RSS series was introduced in 2017. All temperature series are adjusted as new versions are introduced from time to time. This issue is discussed in more detail in Section 7.

The overall temperature variation in the two series (Figures 3 and 4) is similar, but the increase over 1979–2019 is larger for RSS than for UAH. Before the 2017 adjustment of the RSS series, the temperature increase was almost identical for the two series.

(a) UAH
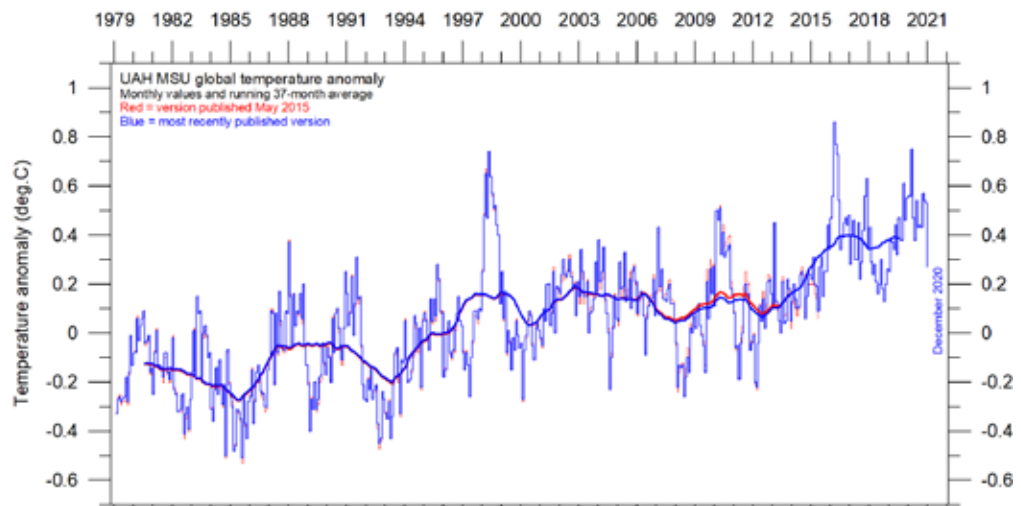
(b) RSS
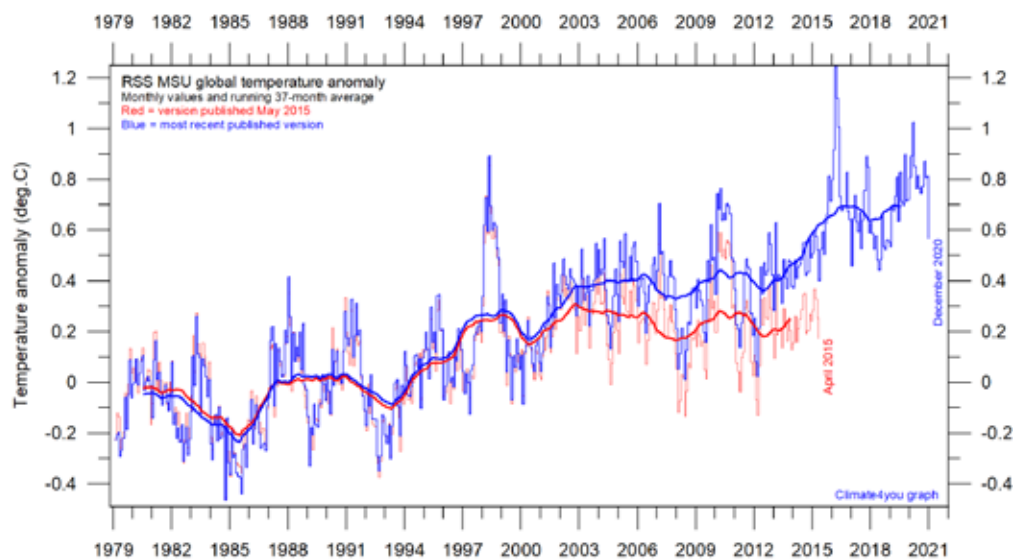
Figure 3: Global monthly average lower troposphere temperatures since 1979.

(a) UAH and (b) RSS. The thick line is the simple running 37-month average, nearly corresponding to a running 3-year average. The 2015 versions of the datasets are shown in red.
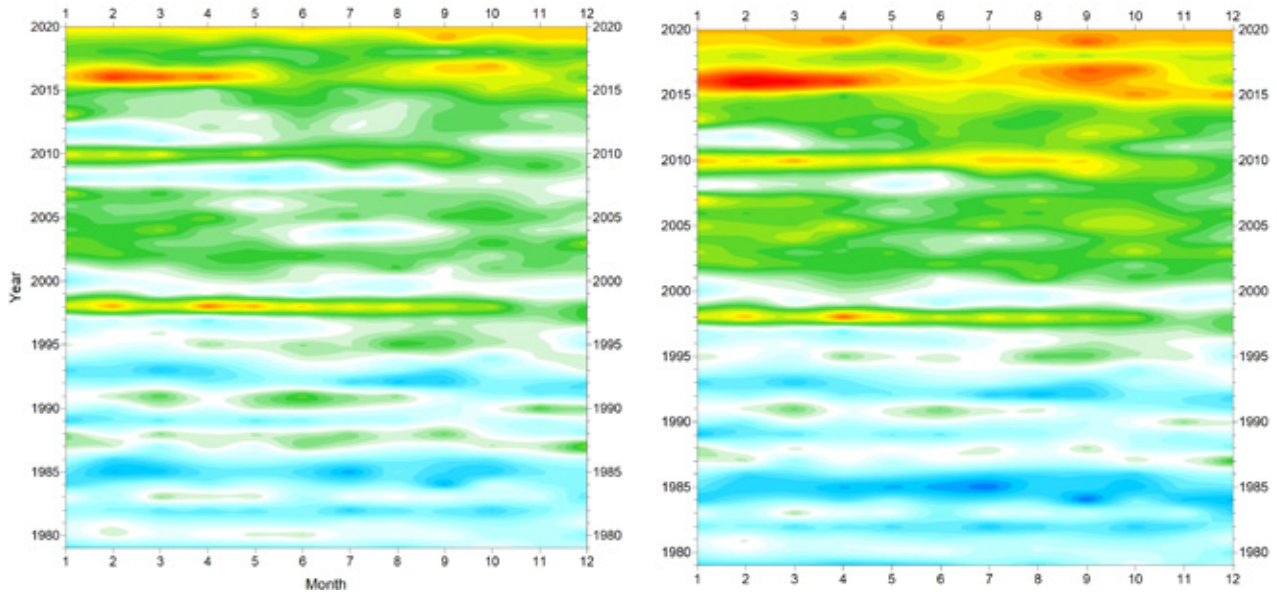
(a) UAH   (b) RSS

Figure 4: Temporal evolution of global lower troposphere temperatures since 1979.

Temperature anomaly versus 1979–2008. The effects of the El Niños of 1998, 2010 and 2015–2016 are clearly visible, as are the tendency for many El Niños to culminate during the Northern Hemisphere winter. As the different temperature databases are using different reference periods, the series have been made comparable by setting their individual 30-year average 1979–2008 as zero value.

4.   Lower troposphere air temperature since 1979: annual means
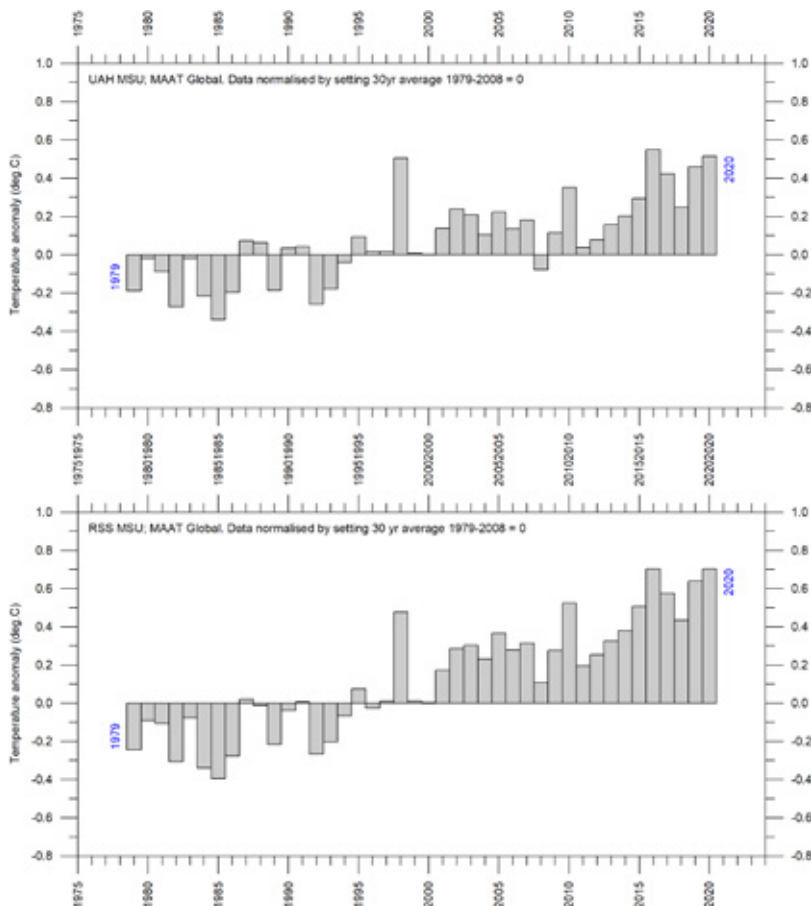
Figure 5: Global mean annual lower troposphere air temperatures since 1979.

Satellite data interpreted by the University of Alabama at Huntsville (UAH), and Remote Sensing Systems (RSS), both in the USA.

7

5. Global monthly surface air temperature since 1979

All three surface air temperature records clearly show the temperature spike associated with the 2015–16 El Niño, the subsequent temperature drop, and the renewed temperature increase due to the moderate 2019–20 El Niño episode (Figure 6).

The comparison between the most recent (December 2020) record and the May 2015 record (red lines in Figure 6) shows that few adjustments have since been introduced in the HadCRUT record, while numerous and relatively large changes have been introduced into both the NCDC and GISS records.

All three surface records, however, confirm the culmination of the recent major El Niño episode in early 2016, the subsequent gradual turning back towards pre-2015 conditions, and the renewed warming in 2019. This development is also demonstrated by Figure 7.

Figure 6: Global mean monthly surface air temperatures since 1979.

(a) HadCRUT4 (b) NCDC (c) GISS. The thick line is the simple running 37-month average, nearly corresponding to a running 3-year average. The 2015 versions are shown in red.
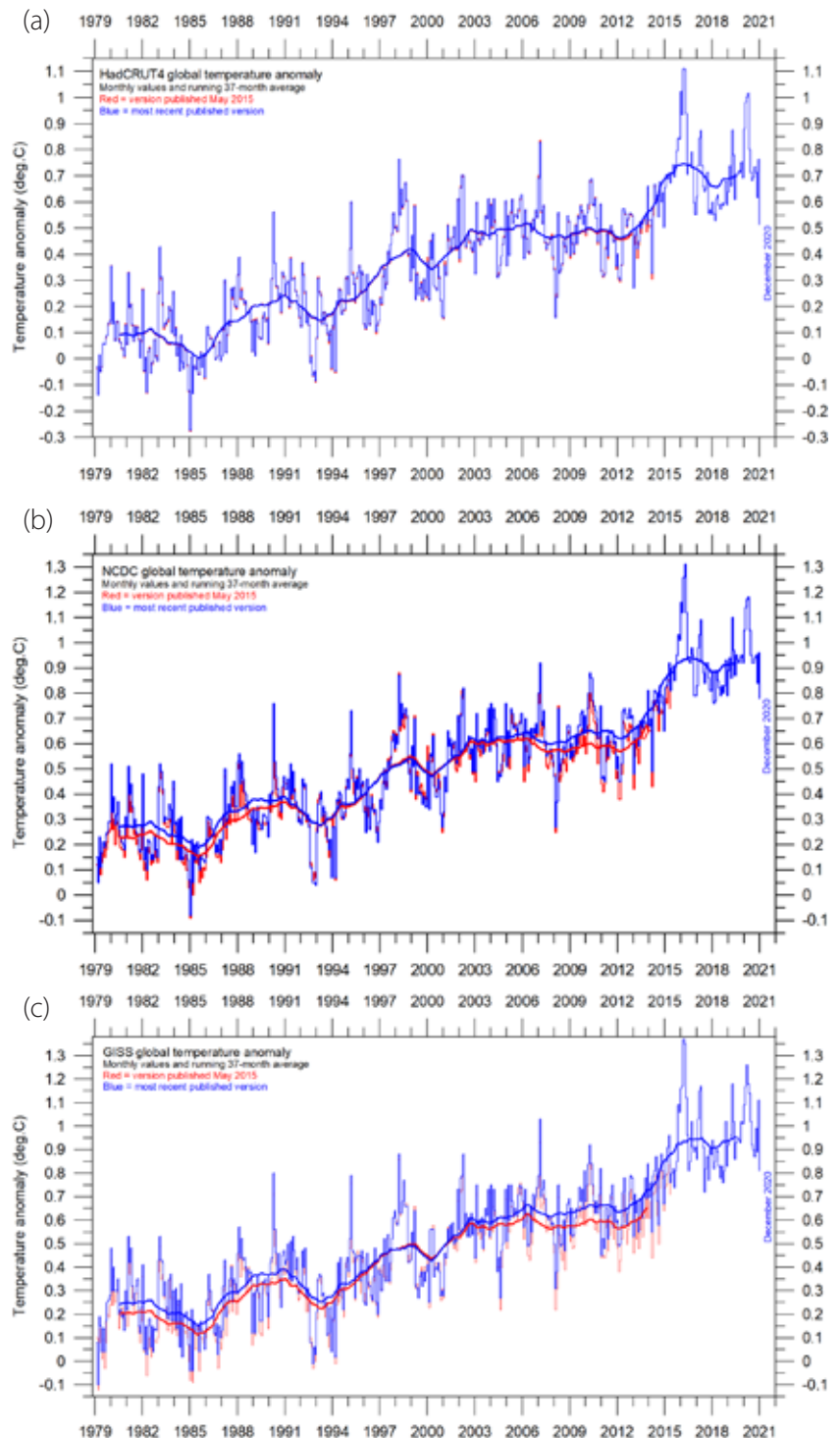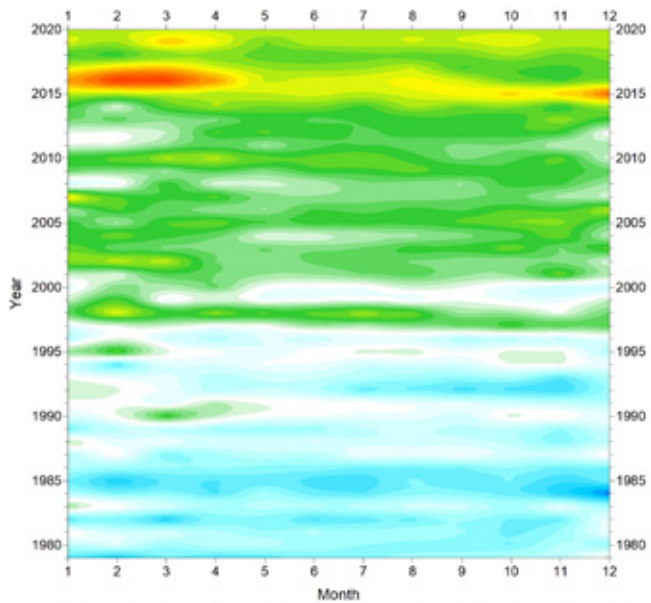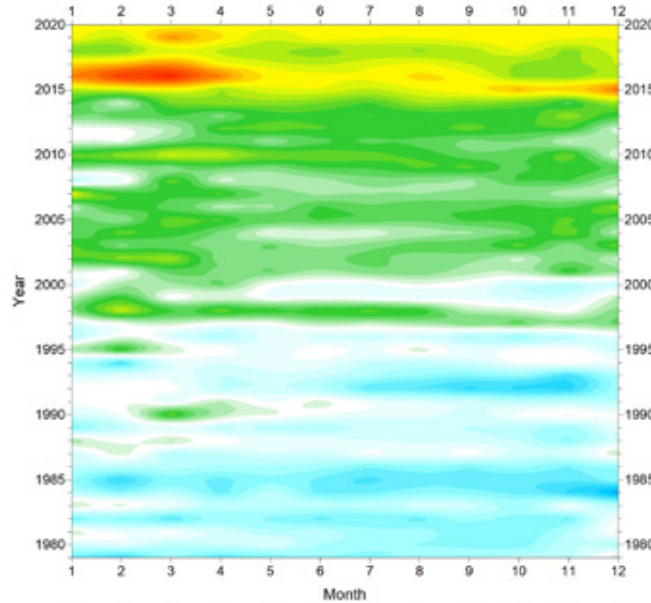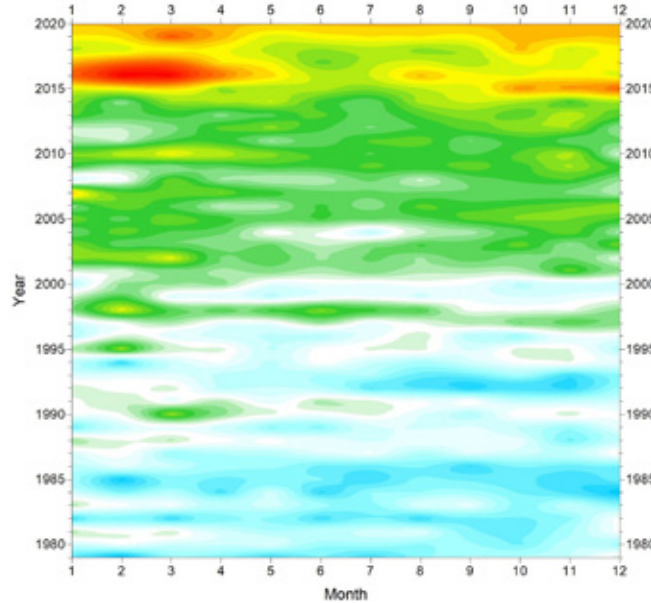
Figure 7: Temporal evolution of global mean monthly surface air temperatures.

(a) HadCRUT4 (b) NCDC (c) GISS. Temperature anomaly (°C) versus 1979–2008.

(a) HadCRUT4

(b) NCDC

(c) GISS

Temperature anomaly (°C)

−0.95 −0.70 −0.45 −0.2 0.05 0.30 0.55 0.80 1.05 1.30
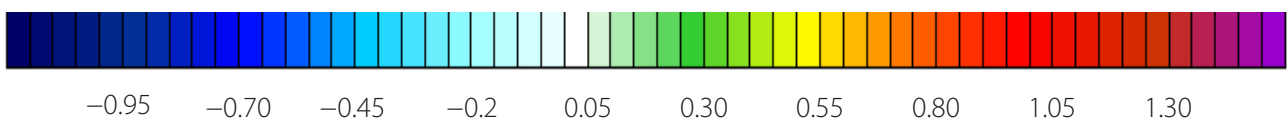
6. Global mean annual surface air temperature

All three average surface air temperature estimates show the year 2016 to be the warmest on record, but also that 2020 was nearly as warm. Both years were highly influenced by El Niño episodes playing out in the Pacific Ocean.
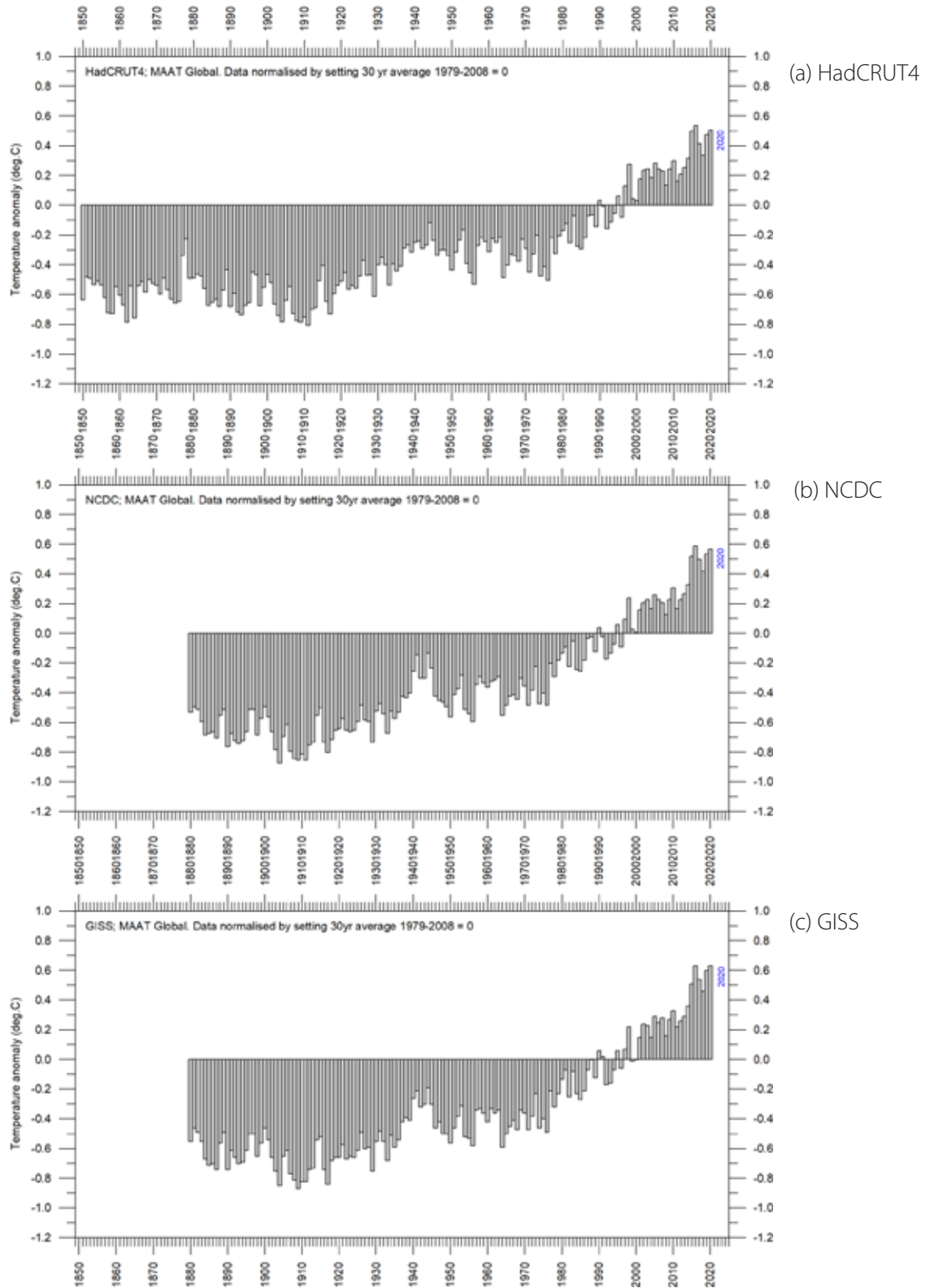
Figure 8: Global mean annual surface air temperatures since 1880.

(a) HadCRUT4 (b) NCDC (c) GISS. Temperature anomaly (°C) versus 1979–2008.

7. Reflections on the margin of error, consistency, and quality of temperature records

According to the various air temperature series, 2020 was a warm year, among the warmest since records began.

The surface temperature records represent a blend of sea-surface data collected from moving ships or by other means, plus data from land stations of partly unknown quality and unknown degree of representativeness for their region. This is because many of the land stations have been moved geographically during their period of operation, instrumentation has been changed, and most stations are influenced by ongoing changes in their surroundings (vegetation, buildings, etc).

The satellite temperature records have their specific problems too, but these are generally of a more technical nature and are therefore probably more readily rectified. In addition, the temperature sampling by satellites is more regular and complete on a global basis, and therefore gives a better representation than the surface records. It is also important to note that the sensors on satellites measure temperature directly by emitted radiation, while most modern surface temperature measurements are indirect, using electronic resistance.

All temperature records are affected by at least three different sources of error, which differ between the individual station records used for calculation of a global average temperature estimate:

- The accuracy is the degree of closeness of measurements to the actual (true) values.

- The precision is the degree to which repeated measurements under unchanged conditions show an identical value, true or not.

- The measurement resolution, which is the smallest change in temperature that produces a response in the instrument used for measurement.

The combination of these three figures is typically what the 'margin of error' attempts to convey for temperature records. The margin of error has been intensively discussed and is probably at least ±0.1℃ for surface air temperature records, and possibly higher. This often makes it statistically impractical to classify any year as having broken a record, as several other years may be within the ±0.1℃ range of the value considered.

Two other issues relating to the margin of error for surface records have not been widely discussed in the same way. First, as an example, it will not be possible to conclude much about the actual value of the December 2020 global surface air temperature before March–April 2021, when data not yet reported (at time of writing in January 2021) will be incorporated in the surface air temperature databases. This is what might be described as the effect of delayed reporting.

The second issue arises from the apparently perpetual changes in monthly and annual temperature values, as adjustments are made to the databases. This means that the average global temperature reported for previous years later will change over time. These ongoing changes to the data appear to have little or nothing to do with delayed reporting of missing values. This is demonstrated by the fact that changes are often made to temperatures recorded far back in time, and even before 1900, in particular by GISS and NCDC. Most likely, such adjustments are the result of alterations in the way average monthly values are calculated, in an attempt to enhance the resulting record.

Figure 9 shows the accumulated effect since May 2008 of such administrative changes in the GISS surface air temperature record, which extends back to 1880. It is important to stress that all surface temperature records appear to be subject to such changes. The overall net effect of the administrative changes introduced in the GISS record since May 2008 is warming of the early and modern part of the record and cooling of the period in between: roughly 1900–1970. Several of the net changes introduced since 2008 are quite substantial, ranging from about +0.15 to −0.15℃.

To illustrate the effect of such changes in
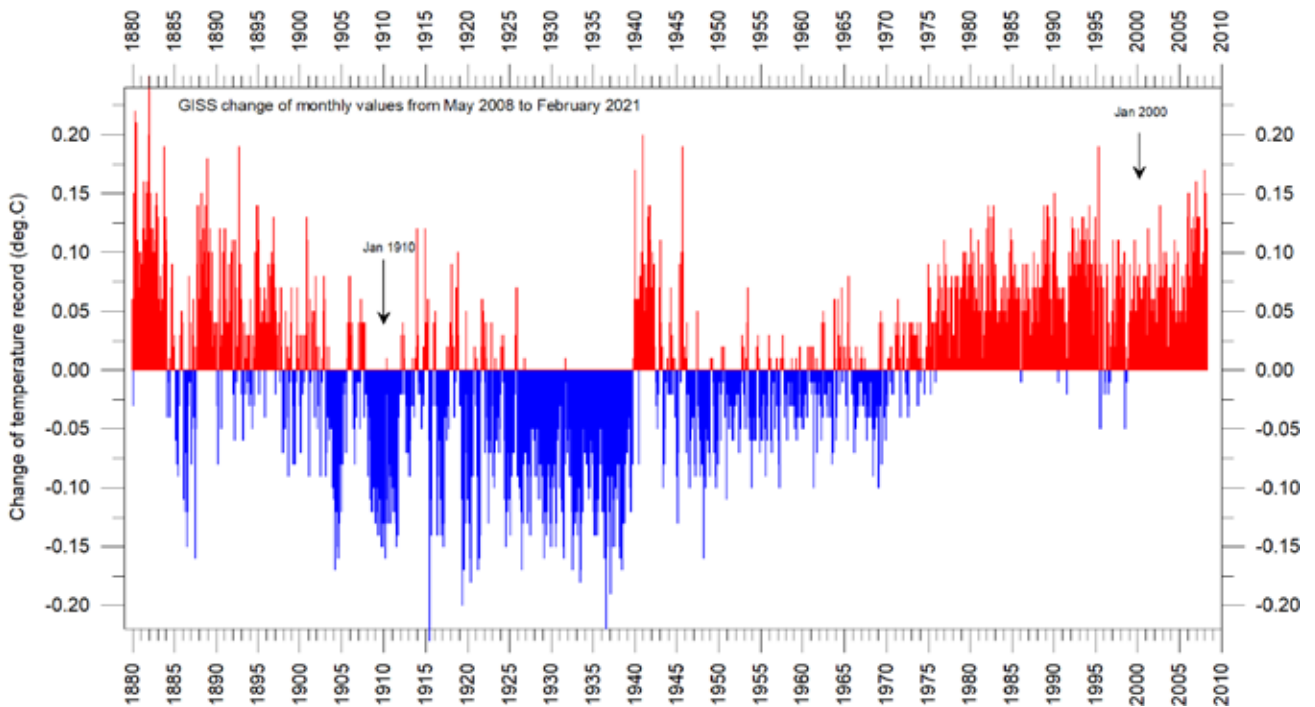
Figure 9: Adjustments since 17 May 2008 in the GISS surface temperature record.

a different way, Figure 10 shows how the GISS values for two months – January 1910 and January 2000 (indicated in Figure 9) – have changed since May 2008. The apparent warming has increased from 0.45°C (as reported May 2008) to 0.66°C (reported in February 2021), or about 47%. In other words, nearly half of the apparent global temperature increases from January 1910 to January 2000 is due to administrative adjustments to the original data made since May 2008. Clearly such adjustments are important when evaluating the overall quality of the various temperature records, along with other standard sources of error. In fact, the magnitude of administrative changes may exceed the formal margin of error.

Everybody interested in climate science should acknowledge the efforts put into maintaining the different temperature databases re-

ferred to in the present report. At the same time, however, it is also important to realise that all temperature records cannot be of equal scientific quality. The simple fact that they differ to some degree shows that they cannot all be correct.

The global mean surface temperature anomaly – with all the errors and uncertainties involved – still stands at the center of most discussions of global warming. For an excellent review of the way the record is constructed and presented, and the implications thereof, the reader is referred to the paper by Lindzen and Christy (2020).

Finally, it may be worth emphasising that a global average temperature will rarely be useful at the regional and local level. Average values may be useful but may also be quite misleading.

Figure 10: Adjustments made since May 2008 to GISS anomalies for the months January 1910 and January 2000.
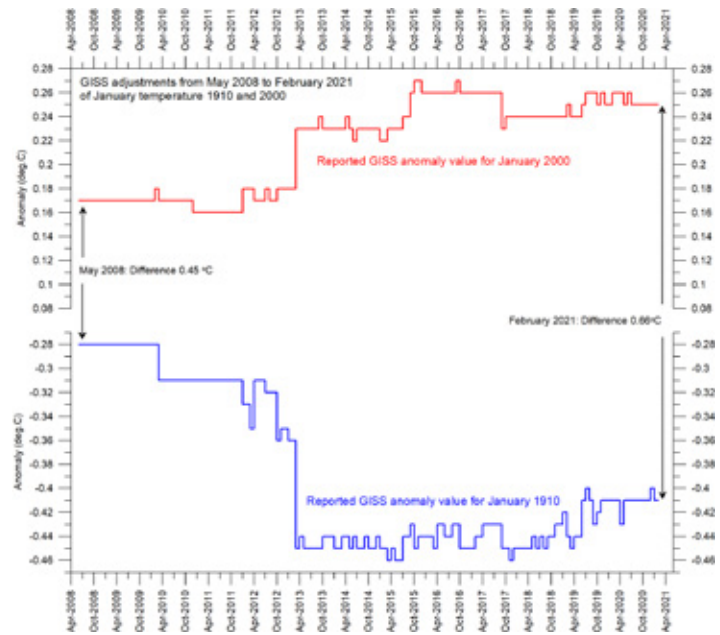
8.   Comparing surface and satellite records

In general, there is fair agreement between the averages of the surface and satellite records, as shown in Figure 11. However, before the major adjustment of the RSS satellite record in 2017, the situation was different, with the average of surface records drifting in a warm direction compared to the satellite records. Again, this illustrates the significance of the ongoing changes made to the individual temperature records.
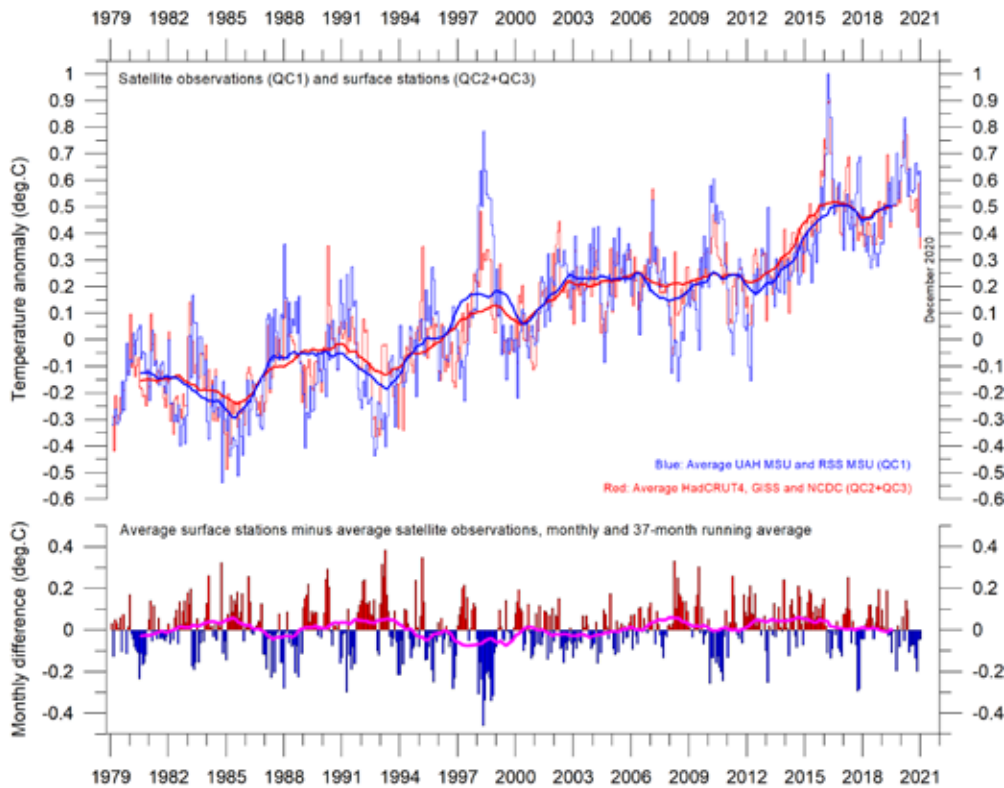
Figure 11: Comparison of surface and satellite records.

Monthly plots for surface (HadCRUT, NCDC and GISS) and satellite (UAH and RSS) records. Thin lines: monthly value; thick lines: 37-month running mean. The lower panel shows the differences between surface and satellite temperatures. Anomalies versus January 1979 to December 2008 mean.

9. Lower troposphere temperature changes over land and oceans

Since 1979, the lower troposphere over land has warmed much more than over oceans. There may be several reasons for this, such as variations in incoming solar radiation, cloud cover, and land use.
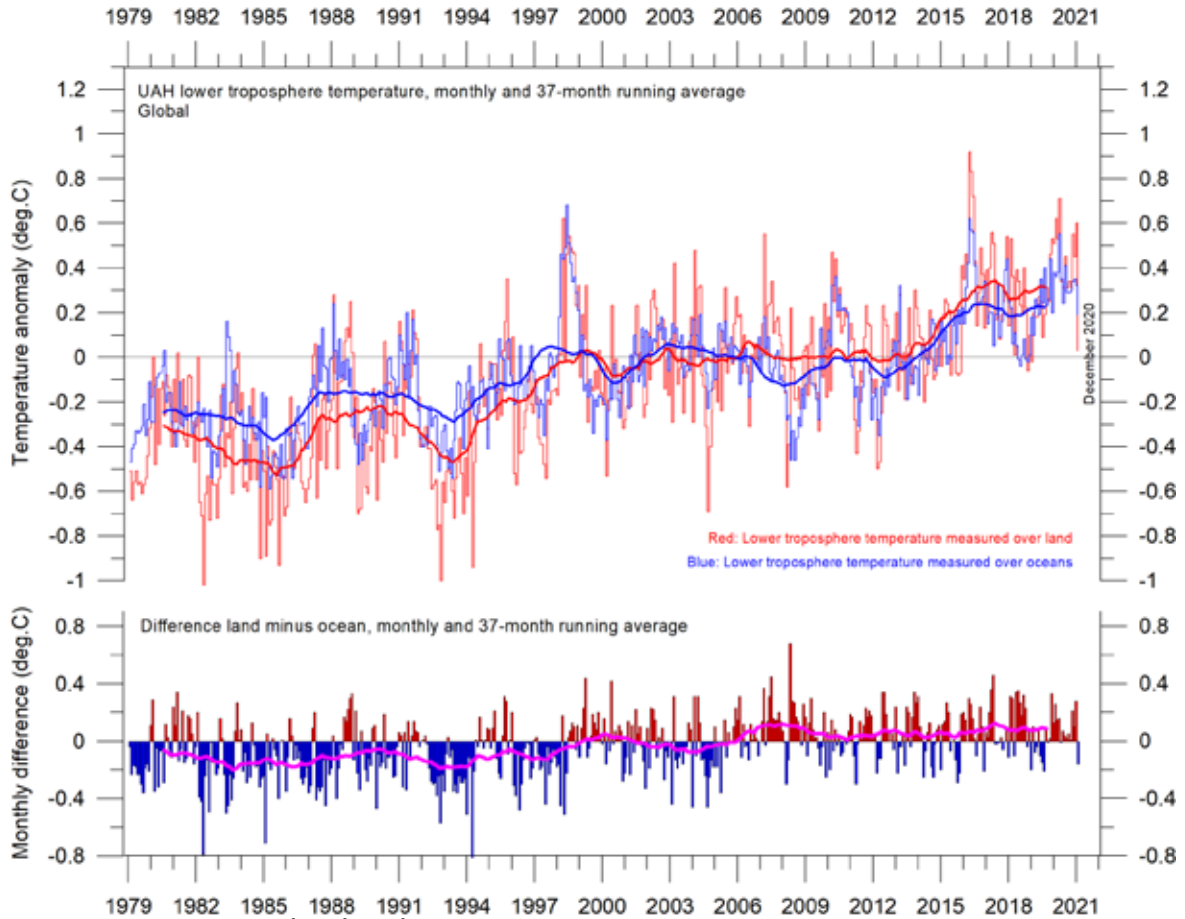
Figure 12: Warming over land and oceans.

Global monthly average lower troposphere temperature since 1979 measured over land and oceans, shown in red and blue, respectively, according to University of Alabama at Huntsville (UAH), USA. Thin lines: monthly value; thick lines: 37-month running mean.

10. Temperature changes at different altitudes

Changes in the vertical temperature profile of the atmosphere (Figure 13) are important because increasing tropospheric temperatures and decreasing stratospheric temperatures are two central features of the hypothesis of warming induced by human emissions of carbon dioxide.

The temperature variations recorded in the lowermost troposphere are generally reflected at higher altitudes, up to about 10 km altitude. The overall temperature plateau since about 2002 is found at all these altitudes, as is the El Niño induced temperature increase in 2015–16.

At high altitudes, near the tropopause, the pattern of variations recorded lower in the atmosphere can still be recognised, but for the duration of the record (since 1979) there has been no clear trend towards higher or lower temperatures.

Higher in the atmosphere, in the stratosphere, at 17 km altitude, two pronounced temperature spikes are visible before the turn of the century. These can both be related to major volcanic eruptions. Ignoring these spikes, until about 1995 the stratospheric temperature record shows a persistent decline, ascribed by

various scientists to the effect of heat being trapped by carbon dioxide in the troposphere below. However, the marked temperature decline in the stratosphere essentially ended around 1995–96, since when temperatures have been largely unchanged. Thus, the stratospheric temperature 'pause' initiated 5–7 years before the similar 'pause' in the lower troposphere. Noteworthy for 2020, however, was a marked, but short-lived, temperature peak, rapidly followed by an equal drop in temperature. By the end of 2020 the stratospheric temperature at 17 km altitude was back to the pre-2020 level.
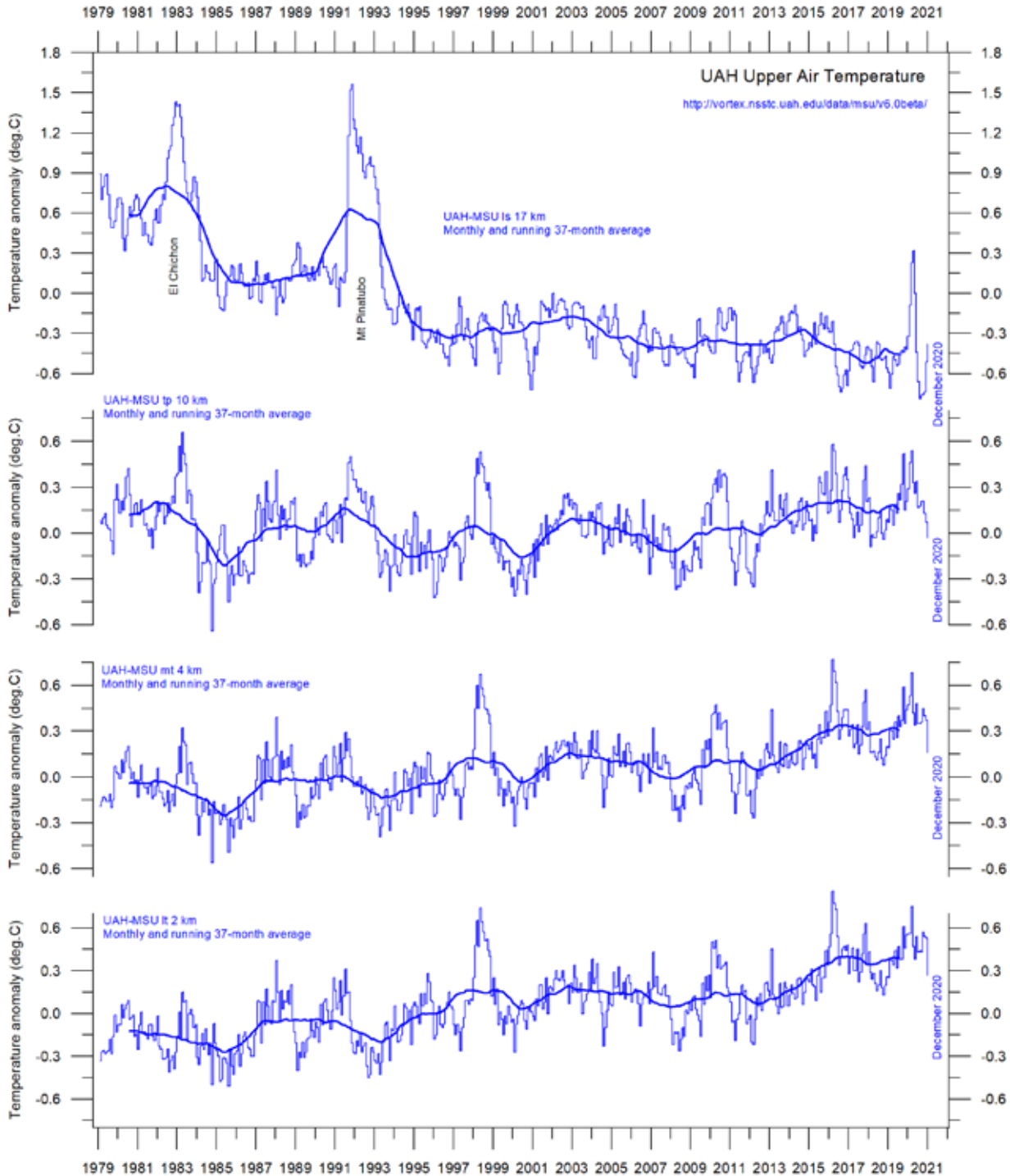
Figure 13: Temperature changes through the atmosphere.

Global monthly average temperature in different altitudes according to University of Alabama at Huntsville (UAH), USA. Thin lines: monthly value; thick lines: 37-month running mean.

11. Atmospheric greenhouse gases: water vapour and carbon dioxide

Water vapour

Water vapour is the most important greenhouse gas in the troposphere. The highest concentration is found within a latitudinal range from 50°N to 60°S. The two polar regions of the troposphere are comparatively dry. Water vapour is a much more important greenhouse gas than carbon dioxide, both because of its absorption spectrum and because of its higher atmospheric concentration.

Figure 14 shows the specific atmospheric humidity to be stable or slightly increasing up to about 4–5 km altitude. At higher levels in the troposphere (about 9 km), the specific humid-

ity has been decreasing for the duration of the record (since 1948), but with shorter variations superimposed on the falling trend. A Fourier frequency analysis (not shown) reveals these changes to be influenced not only by annual variations, but also by a 34.5-year cycle.

The slight, but persistent, decrease in specific humidity at about 9 km altitude is noteworthy, as this altitude roughly corresponds to the level where the theoretical temperature effect of increased atmospheric carbon dioxide is expected initially to play out.
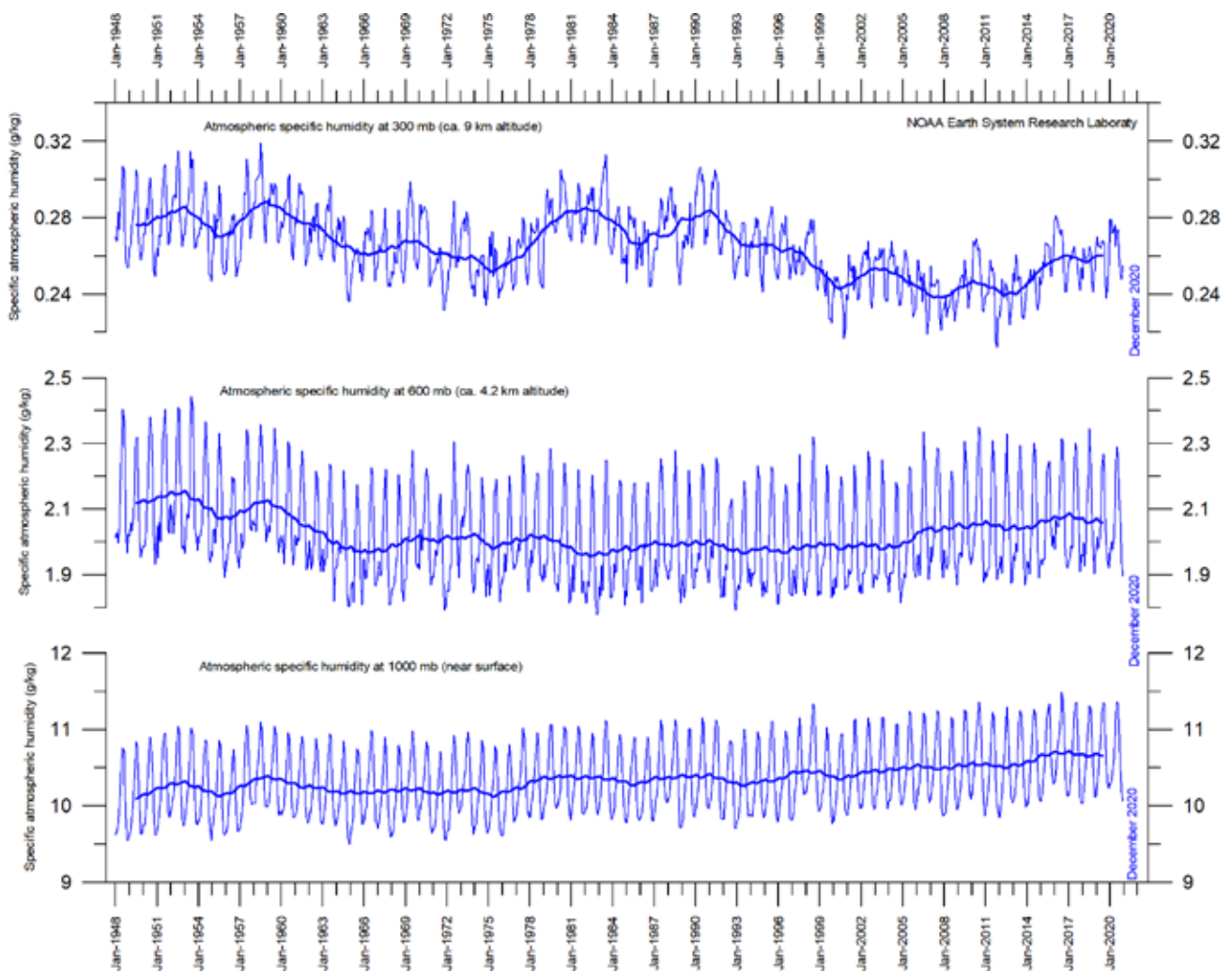
Figure 14: Humidity.

Specific atmospheric humidity (g/kg) at three different altitudes in the troposphere since January 1948. Thin lines: monthly value; thick lines: 37-month running mean. Data source: Earth System Research Laboratory (NOAA).

Carbon dioxide

Carbon dioxide (CO_2) is an important greenhouse gas, although less important than water vapour. For the duration of the record (since 1958), an increasing trend is clearly visible, with an annual cycle superimposed. At the end of 2020, the amount of atmospheric CO_2 was close to 415 parts per million (ppm; Figure 15). Carbon dioxide is usually considered a relatively well-mixed gas in the troposphere. Figure 15 only shows measurements since 1958. Measurements exist for earlier periods, but these are obtained by different techniques (see, e.g. Jaworowski et al. 1992).

The annual change in tropospheric CO_2 has been increasing from about +1 ppm per year in the early part of the record, to about +2.5 ppm per year towards the end of the record (Figure 16). A Fourier frequency analysis (not shown) reveals the annual change of tropospheric CO_2

to be influenced by a cycle of 3.6-years' duration. There is no visible effect of the global COVID-19 lockdown since January 2020 in the amount of atmospheric CO_2.

It is instructive to consider the variation of the annual change rate of atmospheric CO_2 alongside the annual change rates for the global air temperature and global sea surface temperature (Figure 17). All three change rates clearly vary in concert, but with sea surface temperatures leading a few months ahead of the global temperature and change rates for atmospheric CO_2 lagging 11–12 months behind the sea surface temperature change rates.

Figure 18 shows the visual association between annual change of atmospheric CO_2 and La Niña and El Niño episodes, emphasising the importance of oceanographic dynamics for understanding changes in atmospheric CO_2.
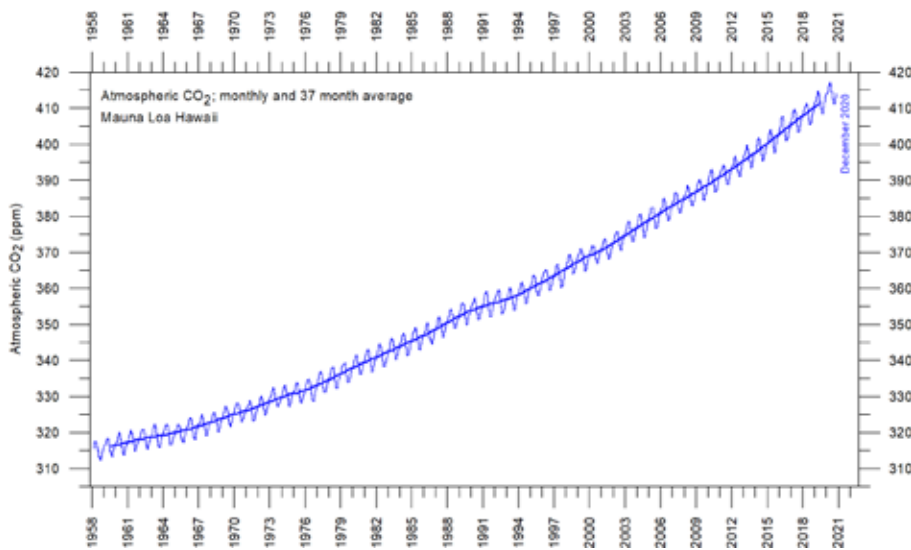
Figure 15: The Mauna Loa CO_2 record

Thin lines: monthly value; thick lines: 37-month running mean.
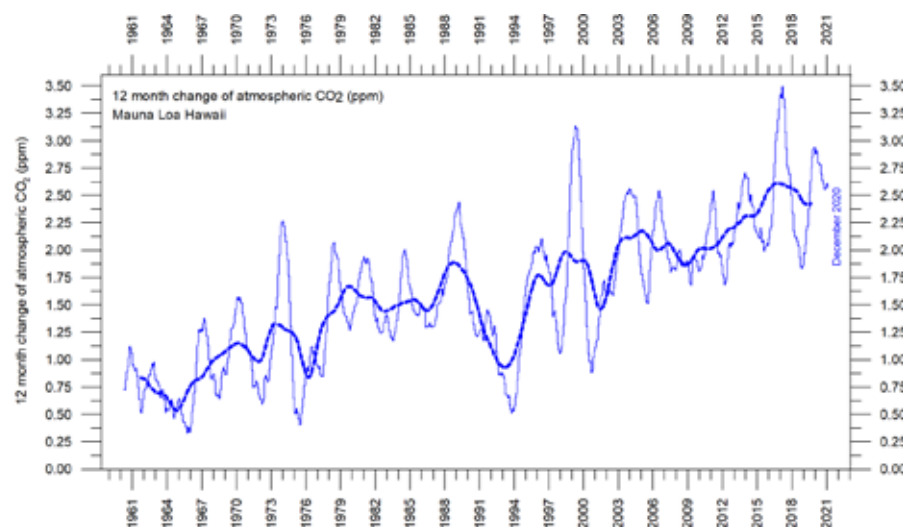
Figure 16: Annual CO_2 change

Difference of two 12-month averages. Thin lines: monthly value; thick lines: 3-year running mean.
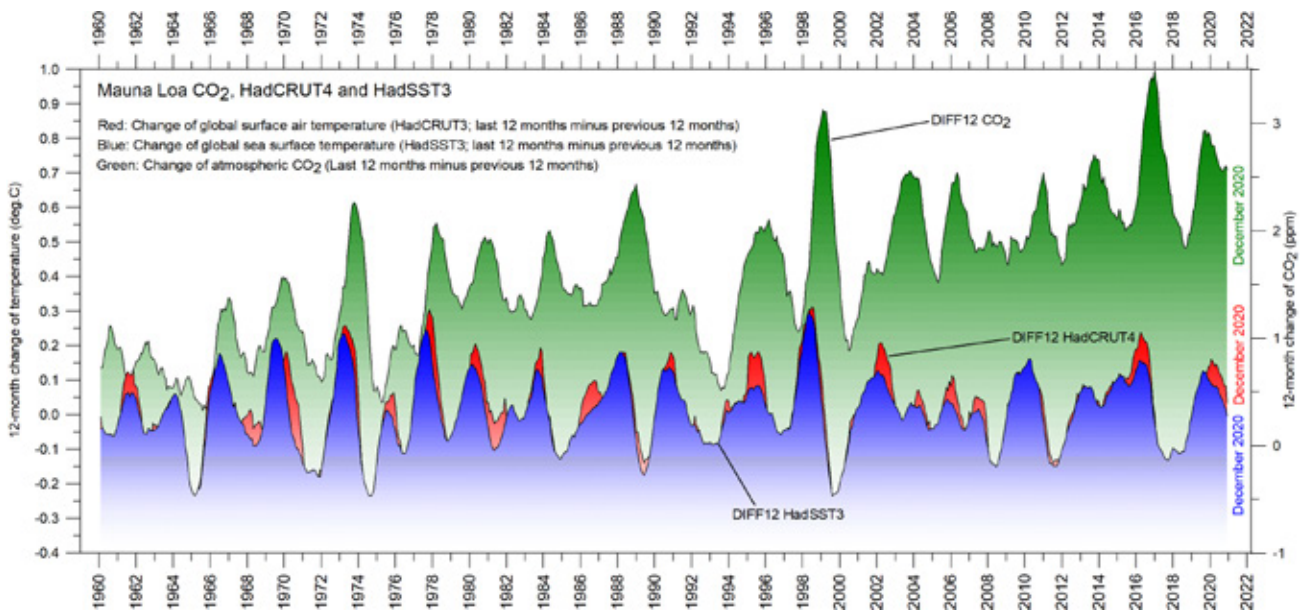
Figure 17: CO$_2$ and temperature

Annual (12-month) change of global atmospheric CO$_2$ concentration (Mauna Loa; green), global sea surface temperature (HadSST3; blue) and global surface air temperature (HadCRUT4; red). All graphs are showing monthly values of DIFF12, the difference between the average of the last 12 months and the average for the previous 12 months for each data series.
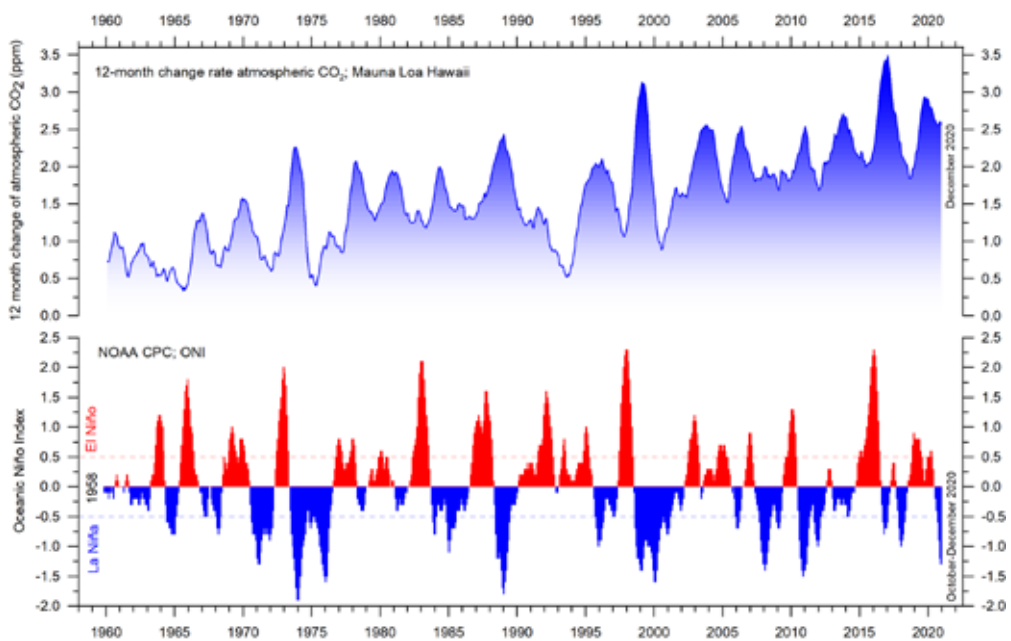
Figure 18: CO$_2$ growth and El Niño

Visual association between annual growth rate of atmospheric CO$_2$ (upper panel) and Oceanic Niño Index (lower panel). See also Figures 16 and 17.

12. Zonal air temperatures

Figure 19 shows that the 'global' warming experienced since 1980 has mainly been a Northern Hemisphere phenomenon, and has mainly played out as a marked change between 1994 and 1999. This apparently rapid temperature change was, however, influenced by the Mount Pinatubo eruption of 1992–93 and the 1997 El Niño episode.

The diagram further reveals how the temperature effects of the strong El Niños in 1997 and 2015–16, as well as the moderate El Niño of 2019, apparently spread to higher latitudes in both hemispheres after some delay. This El Niño temperature effect was, however, mainly recorded in the Northern Hemisphere, and only to a lesser degree in the Southern Hemisphere.
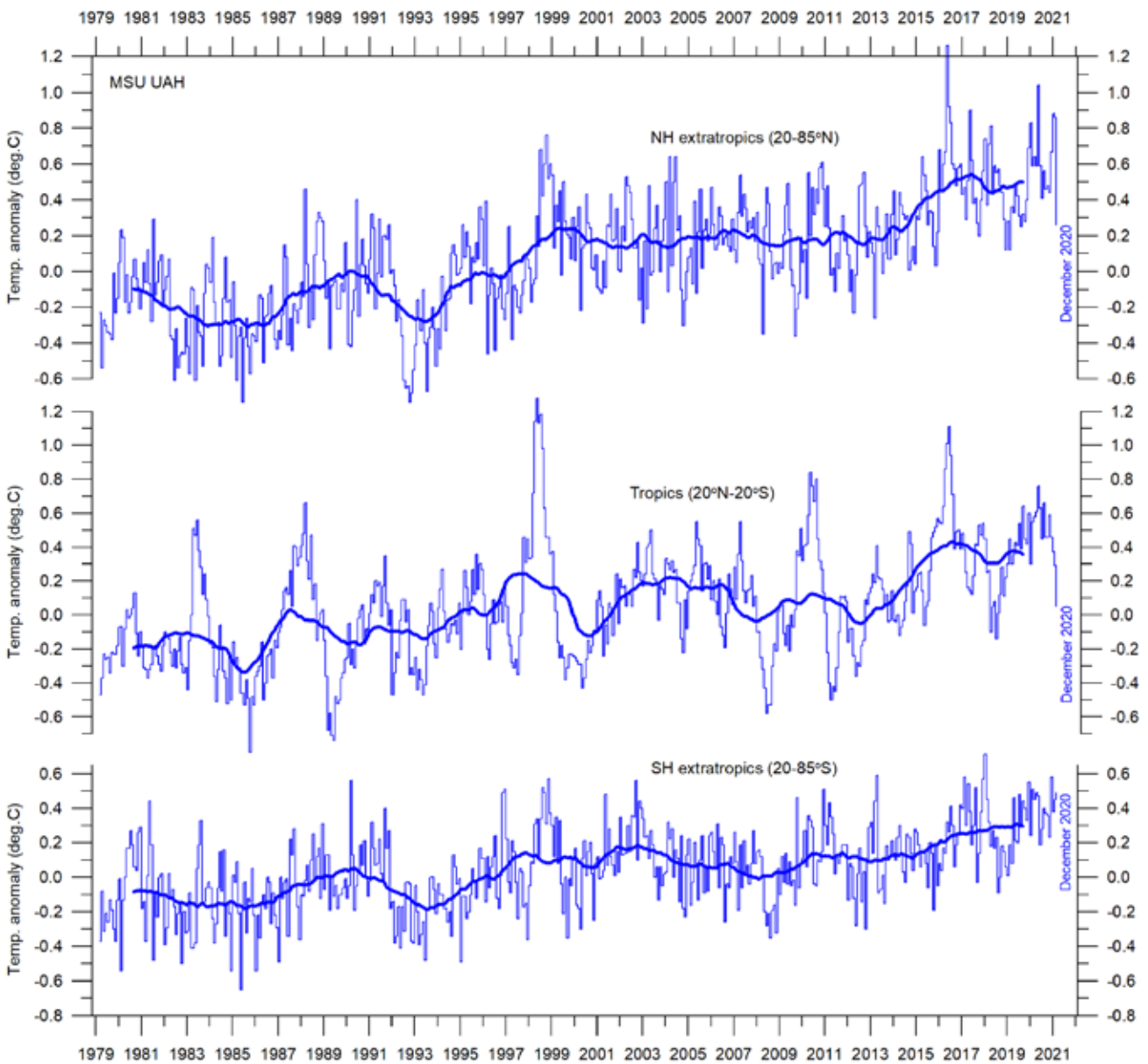
Figure 19: Zonal air temperatures

Global monthly average lower troposphere temperature since 1979 for the tropics and the northern and southern extratropics, according to University of Alabama at Huntsville, USA. Thin lines: monthly value; thick lines: 3-year running mean.

13. Polar air temperatures

In the Arctic, warming mainly took place between 1994 and 1996 (Figure 20). In 2016, however, temperatures peaked for several months, presumably because of oceanic heat given off to the atmosphere during the El Niño of 2015–16 (see also Figure 19) and then advected to higher latitudes. There has been a slight temperature decrease in the Arctic since 2016.

In the Antarctic region, temperatures have remained almost stable since the onset of the satellite record in 1979. In 2016–17, the small temperature peak visible in the monthly record may be interpreted as a subdued effect of the recent El Niño episode.
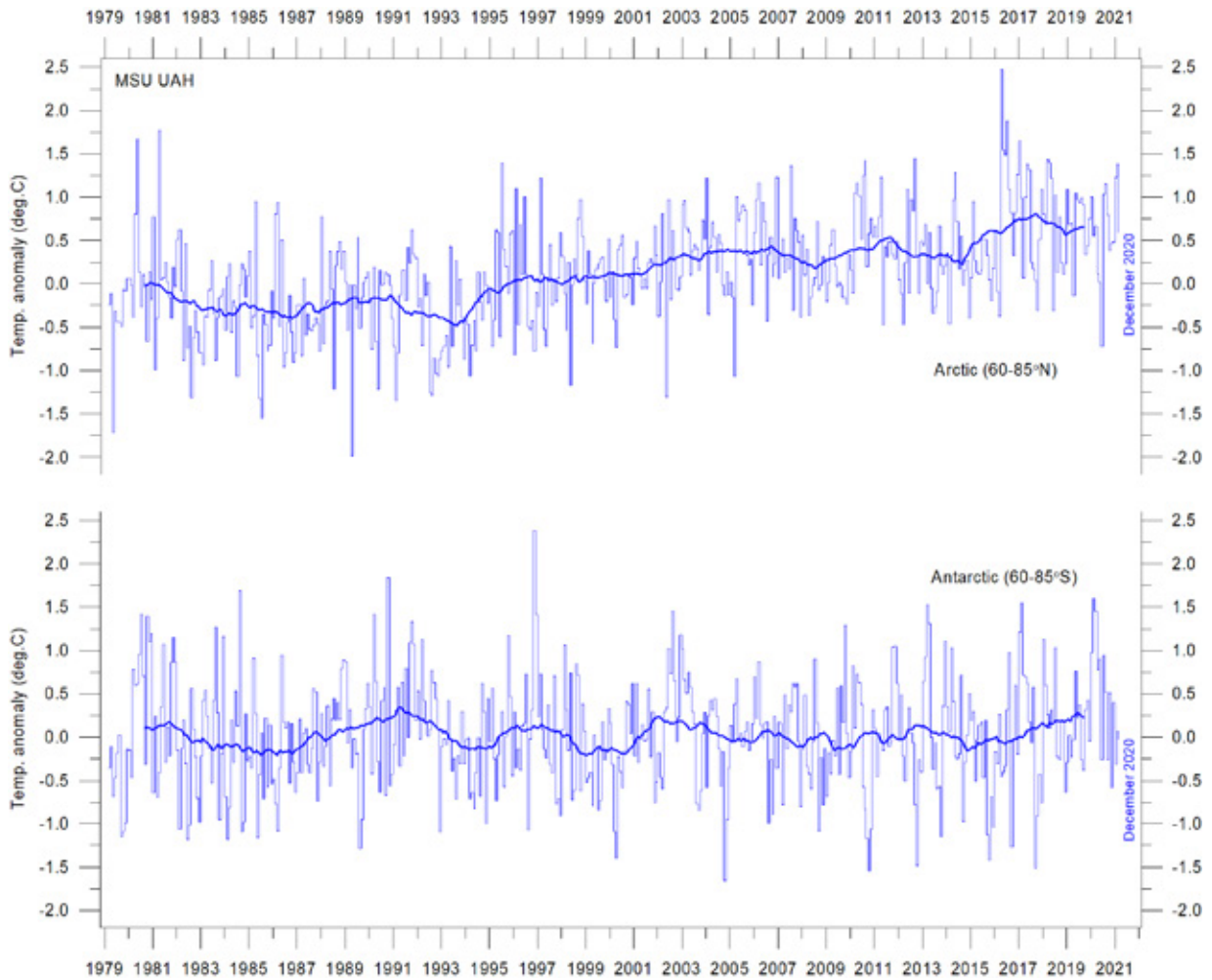
Figure 20: Polar temperatures

Global monthly average lower troposphere temperature since 1979 for the North Pole and South Pole regions, according to University of Alabama at Huntsville, USA. Thick lines are the simple running 37-month average.

14. Sea surface temperature anomalies 2018–2020

Figure 21 shows the nearly neutral sea-surface temperature situation at the end of December 2018, and a nearly neutral situation at the end of 2019, following the moderate El Niño characterising most of that year. Finally, at the end of 2020, the onset of a new La Niña episode is clearly visible in equatorial Pacific Ocean. See also Figure 22, where all El Niño and La Niña episodes since 1950 are displayed.

The 2015–16 El Niño episode was among the strongest since the beginning of the record in 1950. Considering the entire record, however, recent variations between El Niño and La Niña episodes do not appear abnormal in any way.
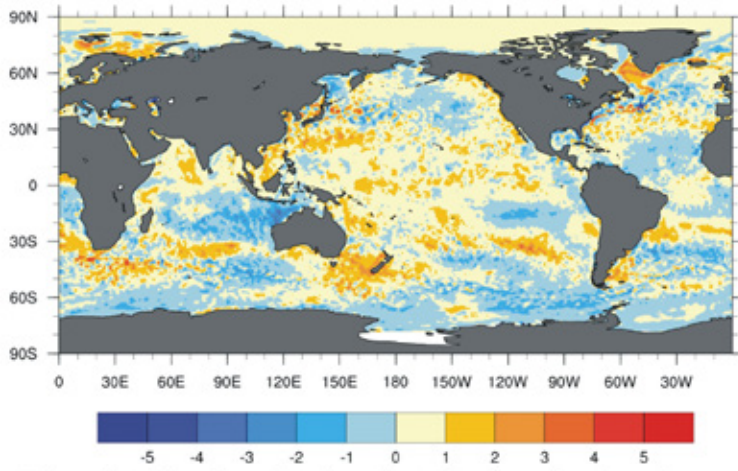
2018

Figure 21: Sea surface temperature anomalies

December sea surface temperature anomalies 2018, 2019 and 2020, (°C). Reference period: 1977–1991. Dark grey represents land areas. Map source: Plymouth State Weather Center. Please note the change of colour scale in 2019.
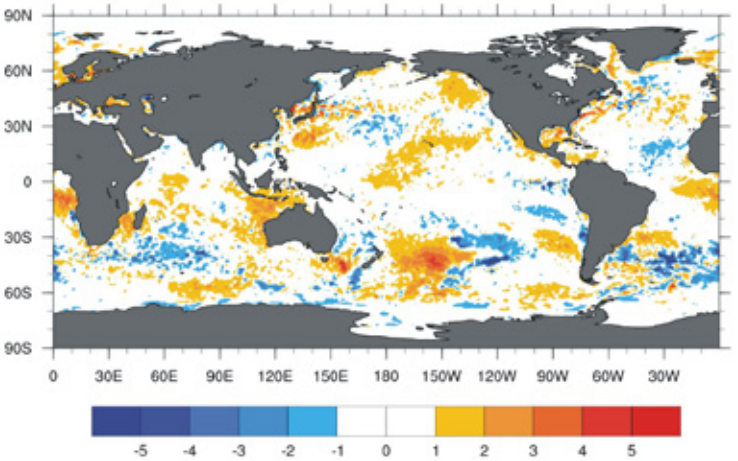
2019
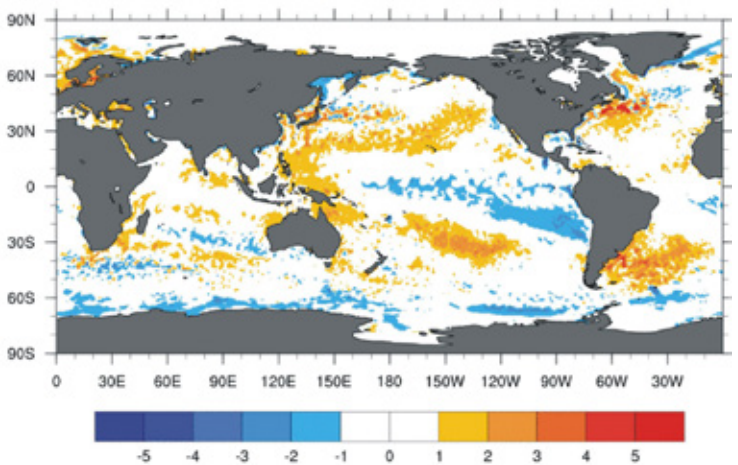
2020
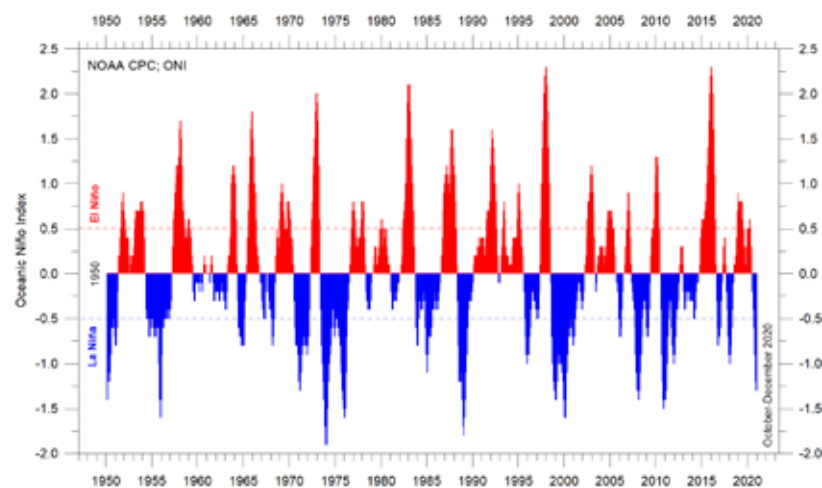
Figure 22: The El Niño index

Warm and cold episodes for the Oceanic Niño Index (ONI), defined as 3 month running mean of ERSST.v5 SST anomalies in the Niño 3.4 region (5°N-5°S, 120°-170°W). Anomalies are centred on 30-year base periods updated every 5 years.

15. Global ocean average temperatures to 1900 m depth

The Argo Program (Roemmich and Gilson 2009) now has achieved 15 years of global coverage, growing from a relatively sparse array of 1000 profiling floats in 2004 to more than 3900 in January 2021, covering most large oceans. Figure 23, based on observations by Argo floats, shows that, on average, the temperature of the global oceans down to 1900 m depth has been increasing since about 2010. It is also seen that since 2013 the increase has been predominantly due to changes occurring near the Equator, between 30°N and 30°S. In contrast, for the circum-Arctic oceans, north of 55°N, depth-integrated ocean temperatures have been decreasing since 2011. Near the Antarctic, south of 55°S, temperatures have essentially been stable. At most latitudes, a clear annual rhythm is seen.
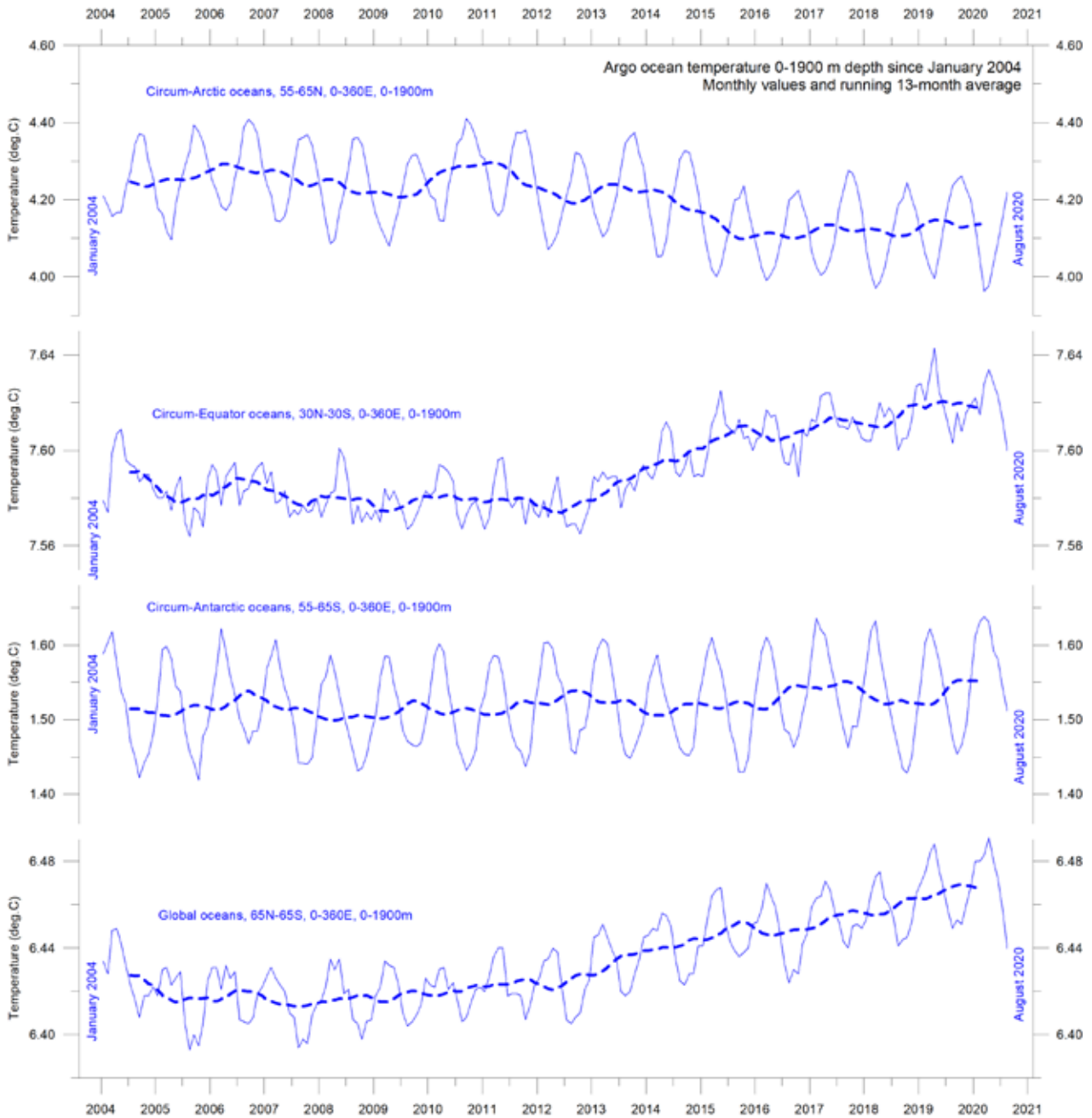
Figure 23: Ocean temperatures to 1900 m

Average ocean temperatures January 2004–August 2020 at 0–1900 m depth in selected latitudinal bands, using Argo data. The thin line shows monthly values, and the thick dotted line shows the running 13-month average. Source: Global Marine Argo Atlas.

16. Global ocean temperatures at different depths

Figure 24 shows global average oceanic temperatures at different depths. An annual rhythm can be traced to about 100 m depth. In the uppermost 100 m, temperatures have increased since about 2011. At 200–400 m depth, temperatures have exhibited little change during the observation period.

For depths below 400 m, however, temperatures are again seen to have increased over the observational period. Interestingly, this increase first commenced at 1900 m depth around 2009, and has been gradually spreading upwards. At 600 m depth, the present temperature increase began around 2012; that is, about three years after it appeared at 1900 m depth. The timing of these changes shows that average temperatures in the upper 1900 m of the oceans are not only influenced by conditions playing out at or near the ocean surface, but also by processes operating at greater depths. Thus, part of the present ocean warming appears to be due to circulation features operating at greater depths than 1900 m and not directly related to processes operating at or near the surface.
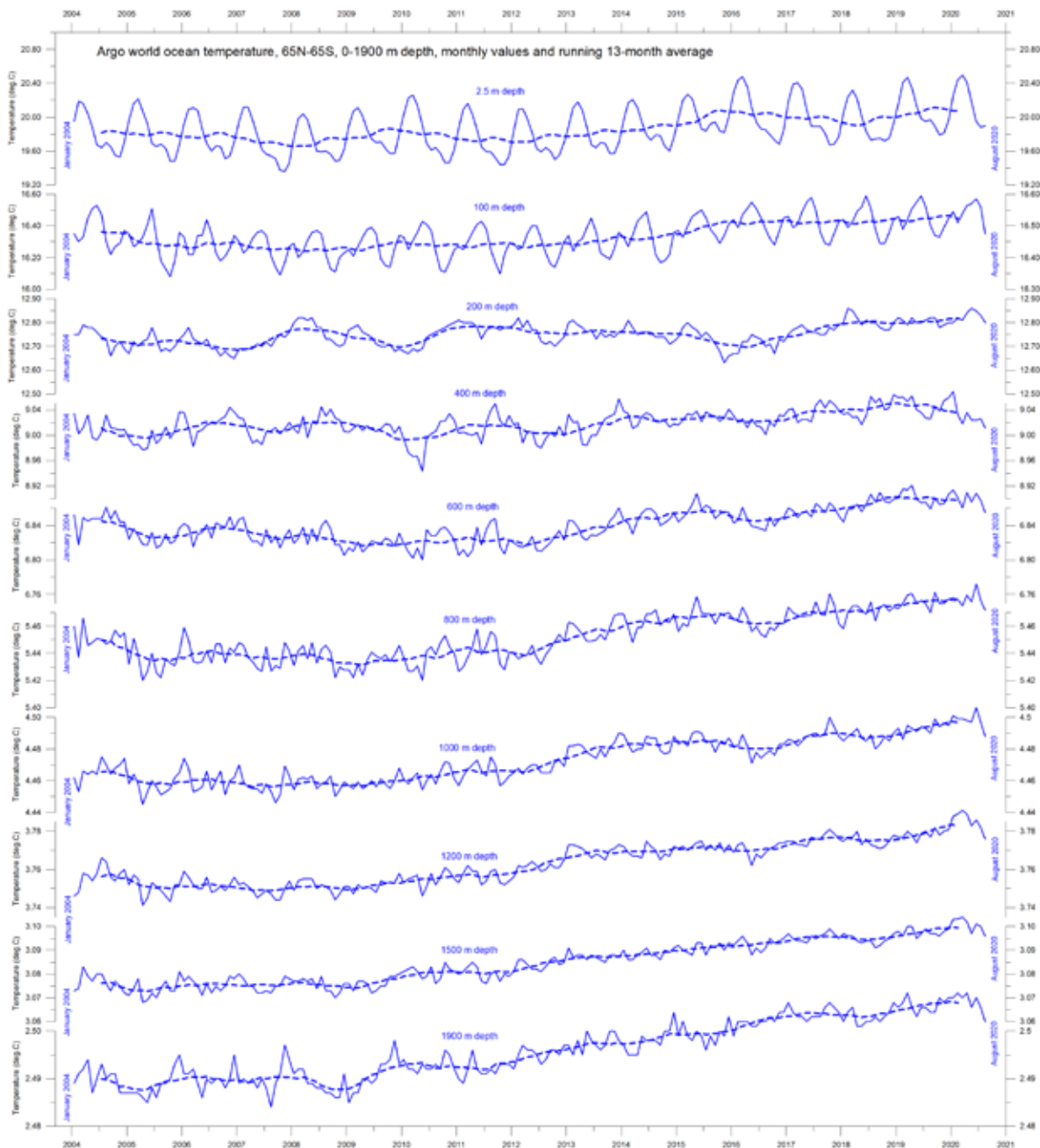
Figure 24: Ocean temperatures at different depths

Ocean temperatures January 2004–August 2020 at different depths between 65°N and 65°S, using Argo data. The thin line shows monthly values, and the dotted line shows the running 13-month average. Source: Global Marine Argo Atlas.

This development is also seen in Figure 25, which shows the net change of global ocean temperature at different depths, calculated as the net difference between the 12-month averages of January–December 2004 and September 2019 –August 2020, respectively. The largest net changes are seen to have occurred in the uppermost 200 m of the water column. However, average values, as used here, although valuable, also hide many of the interesting regional details seen in Figure 26.
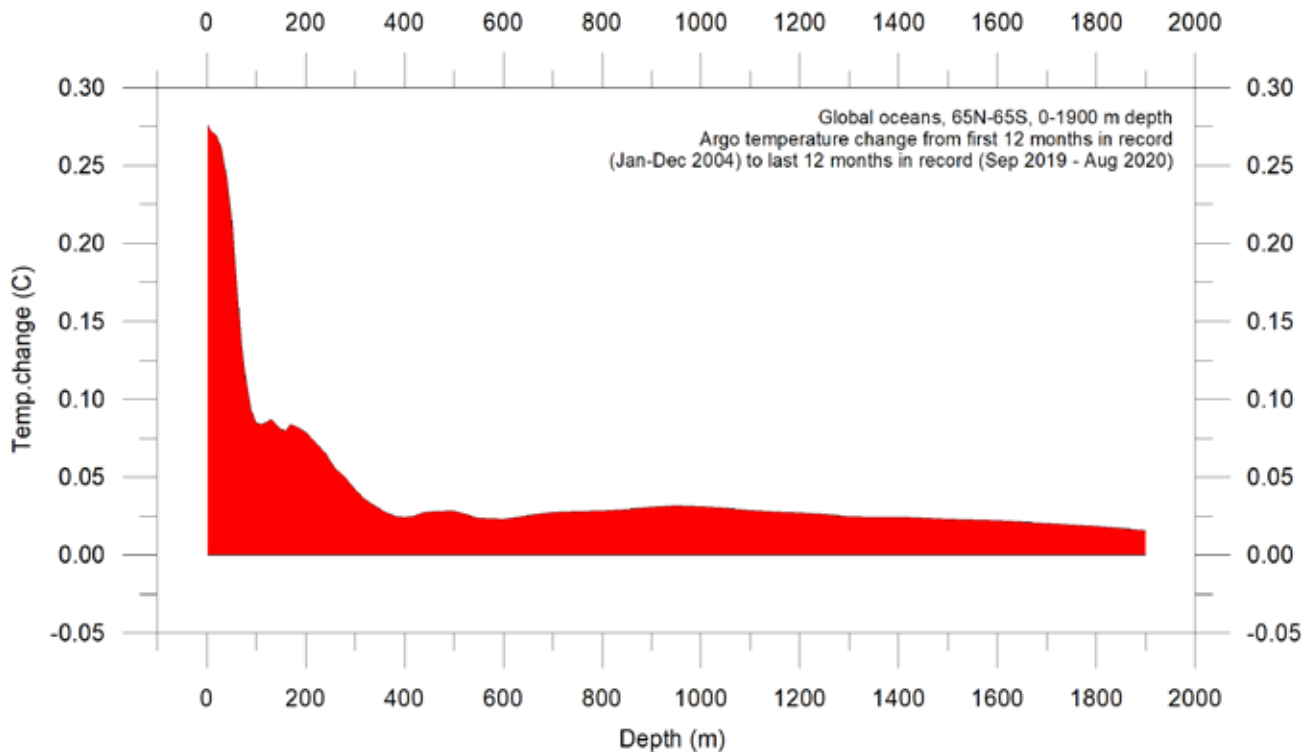
Figure 25: Temperature changes 0–1900 m

Global ocean net temperature change since 2004 from surface to 1900 m depth, using Argo-data. Source: Global Marine Argo Atlas.

17.   Regional ocean temperature changes, 0–1900 m depth

Figure 26 shows the latitudinal variation of oceanic temperature net changes between January–December 2004 and September 2019–August 2020, for various depths, calculated as in the previous diagram. The three panels show the net change in Arctic oceans (55–65°N), Equatorial oceans (30N–30°S), and Antarctic oceans (55–65°S), respectively.

The global surface net warming displayed in Figure 25 affects the Equatorial- and Antarctic oceans, but not the Arctic oceans (Figure 26). In fact, net cooling is pronounced down to 1400 m depth for the northern oceans. However, a major part of Earth's land areas is in the Northern Hemisphere, so the surface area (and volume) of 'Arctic' oceans is much smaller than the 'Antarctic' oceans, which in turn is smaller than the 'Equatorial' oceans. In fact, half of the planet's surface area (land and ocean) is located between 30°N and 30°S.

Nevertheless, the contrast in net temperature changes seen in 2004–2020 for the different latitudinal bands is instructive. For the two polar oceans, the Argo data appears to demonstrate the existence of a bi-polar seesaw, as described by Chylek et al. (2010). It is no less interesting that changes in near-surface ocean temperatures in the two polar oceans contrasts with changes in sea-ice levels in the two polar regions (see Section 25).
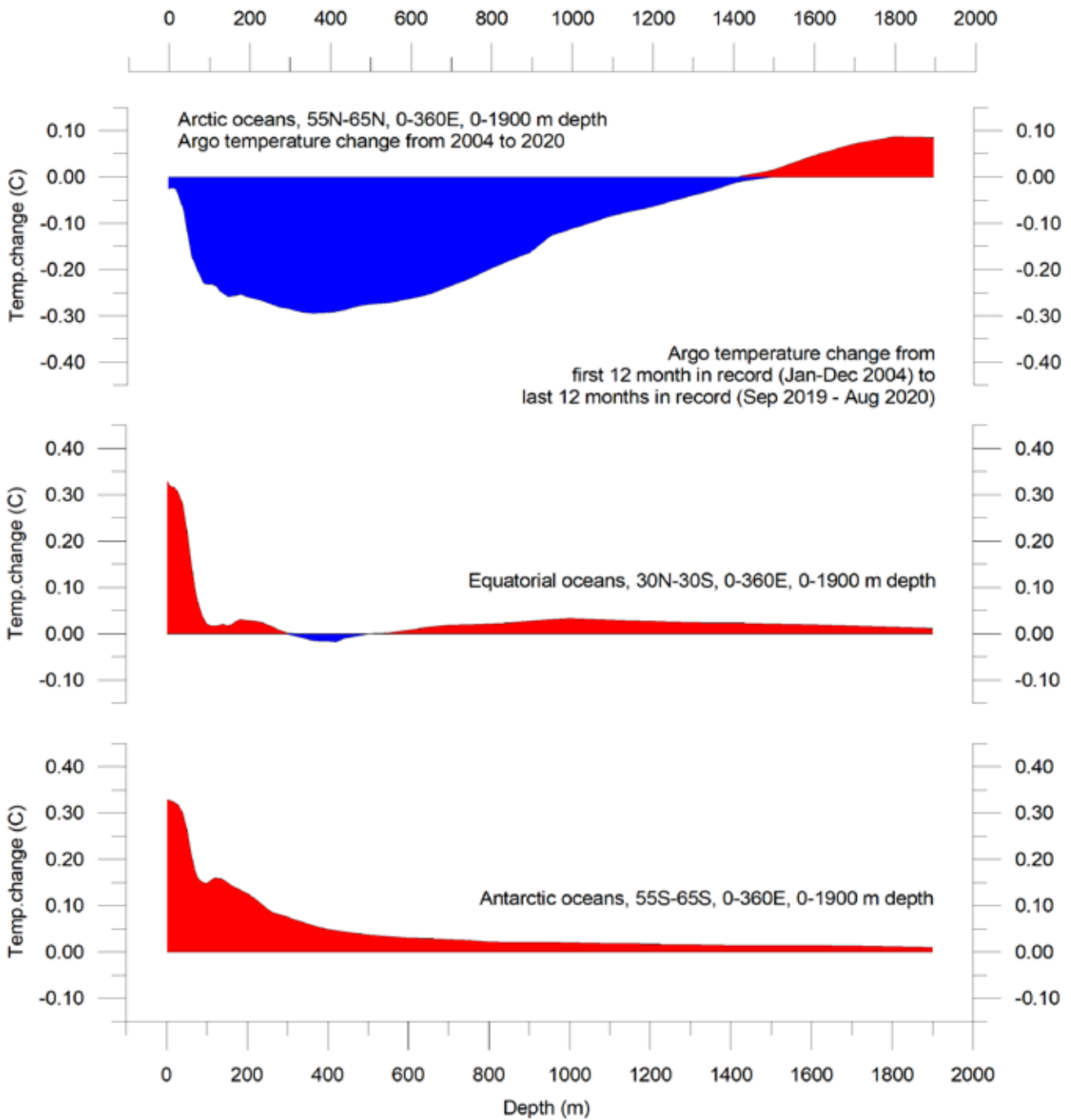
Figure 26: Temperature changes 0–1900 m

Global ocean net temperature change since 2004 from surface to 1900 m depth, using Argo-data. Source: Global Marine Argo Atlas.

18. Ocean temperature net change 2004–2020 in selected sectors

This section considers temperature changes along two longitudinal profiles – 20°W and 150°W, roughly corresponding to the Atlantic and Pacific Oceans respectively – and one latitudinal profile, corresponding to the North Atlantic Current. The locations of the profiles are shown in Figure 27.

Figure 27: Location of the three profiles

Average annual mean net surface solar radiation (W/m²), and the location of three profiles shown and discussed below.

Atlantic profile

Figure 28a shows net temperature changes 2004–2019 along 20°W. To prepare the diagram, 12-month average ocean temperatures for 2019 were compared to annual average temperatures for 2004, representing the initial 12 months of the Argo record. However, the Argo record is now updated to August 2020, and to enable insight into the most recent changes, the 12-month net change from September 2019 to August 2020 is shown in Figure 28b. Warm colours indicate net warming and blue colours indicate cooling. Due to the spherical shape of

the Earth, northerly and southerly latitudes represent only small ocean volumes compared to latitudes near the Equator. With this reservation in mind, Figure 28 nevertheless reveals several interesting features.

The most prominent feature in the Atlantic profile for 2004–2019 is a marked net cooling
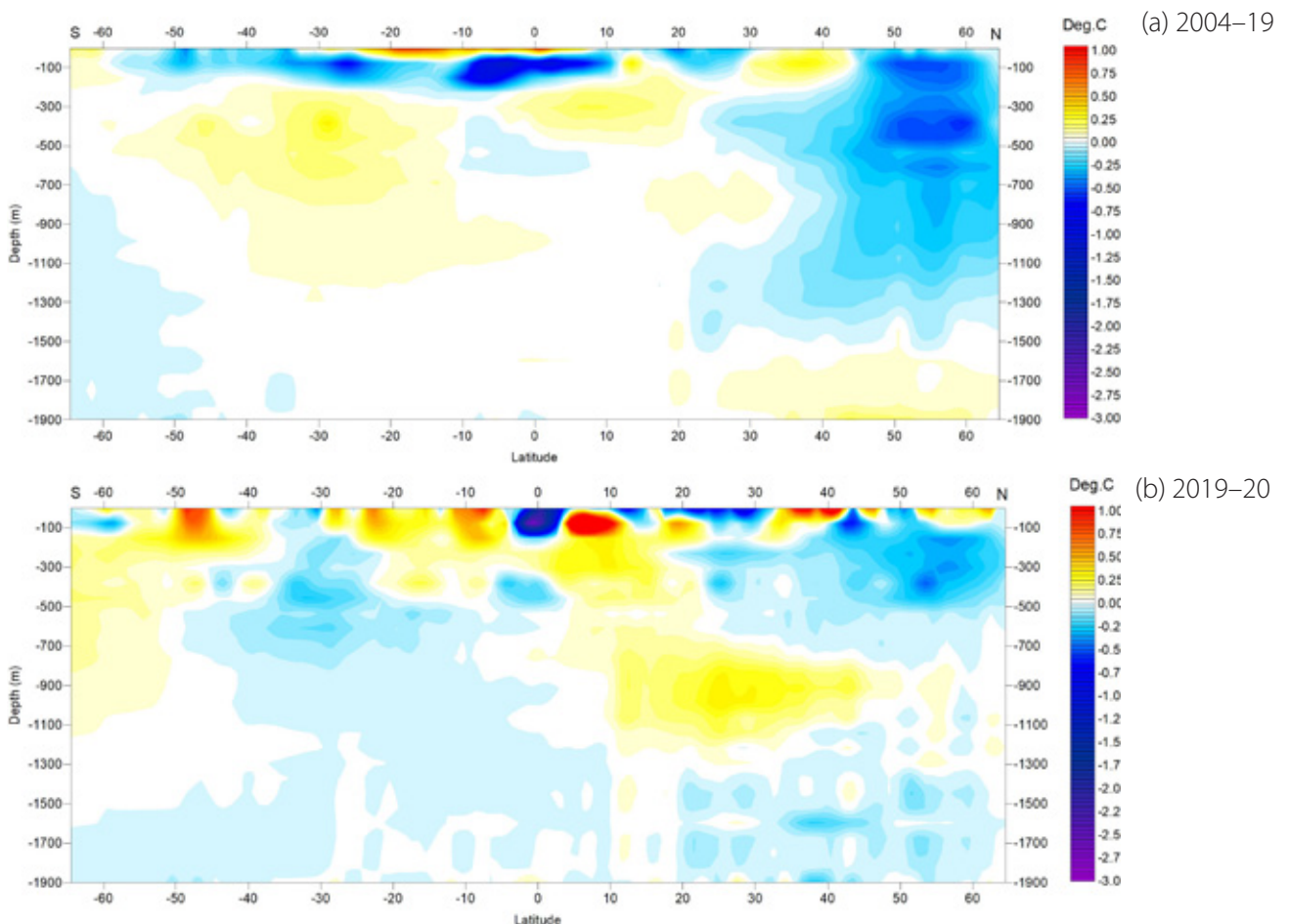
Figure 28: Temperature change along Atlantic profile, 0–1900 m

(a) 2004–2019 and (b) Sept 19–Aug 20. See Figure 27 for geographical location of transect. Data source: Global Marine Argo Atlas.

26

at the surface north of the Equator, especially north of 45°N, where deeper layers (down to 1500 m depth) are involved. At and south of the Equator, net warming dominates at the surface, although net cooling dominates at 50–300 m depth. The maximum Atlantic Ocean net warming for 2004–2019 has taken place between 5°N and 25°S, affecting shallow waters to about 50 m. Warming also affects latitudes between 10°S and 45°S, between 200 and 1200 m depth.

The temperature changes over the last 12 months (Figure 28b) have a more complicated pattern, especially near the surface. However, the South Atlantic warming at depth appears to have weakened over the last 12 months, while the North Atlantic cooling appears to be continuing, with the exception of depths between 800 and 1100 m.

North Atlantic Current profile

The temperature dynamics across the North Atlantic Current, just south of the Faroe Islands, are particularly interesting, as this area is important for weather and climate in much of Europe. This is shown in Figure 29, with temperatures higher than 9°C represented by shades of red.

This time series, although still relatively short, displays some interesting dynamics. The prevalance of warm water (above 9°C) apparently peaked in early 2006, and then fell until 2016. Since then, the trend has partially reversed. The change from peak to trough, playing out over approximately 11 years, might suggest the existence of an approximately 22-year cycle, but we will have to wait until the Argo series is longer before drawing conclusions.

Figure 30 shows the same data processed into a depth-integrated average ocean temperature.

Figure 29: Temperature change along North Atlantic Current profile, 0–800 m

See Figure 27 for geographical location of transect. Data source: Global Marine Argo Atlas.
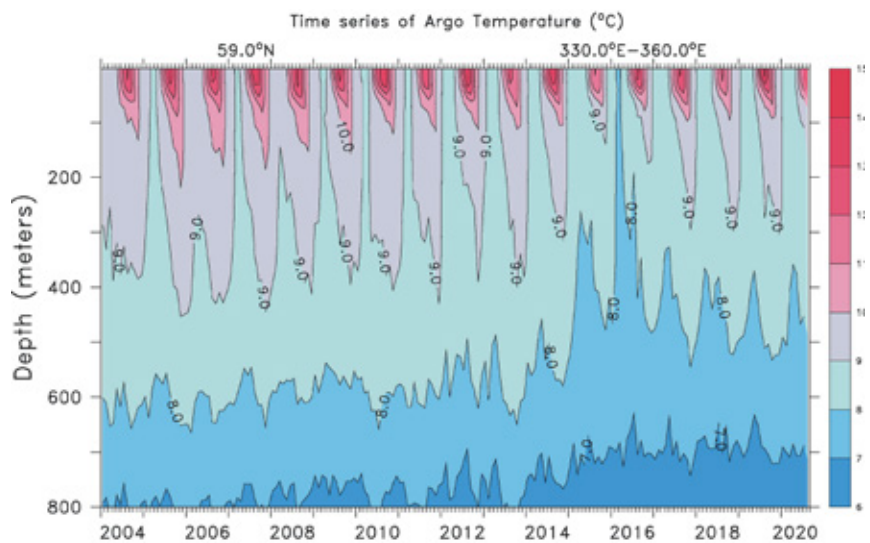
Figure 30: Depth-integrated temperature for the North Atlantic Current profile

See Figure 27 for geographical location of transect. Data source: Global Marine Argo Atlas.
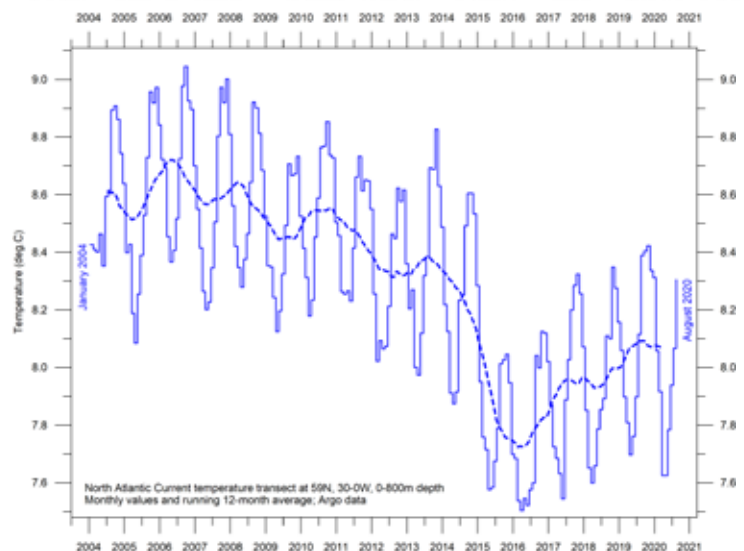
Pacific profile

Figure 31 shows equivalent data along the Pacific profile at 150°W. One interesting feature for 2004–2019 (Figure 31a) is a slight net cooling affecting nearly all water depths down to 1900 m south of 55°S, contrasting with overall net warming down to 1000 m depth north of 55°S. Net warming has been especially prominent between 40°N and 60°N, down to 200 m depth. In contrast, net cooling characterises depths between 100 and 500 m between 5°S and 30°N, and between 20°S and 30°S.

During the last 12 months (Figure 31b), cooling is seen to dominate all depths between 45°S and 30°N. At least part of this recent temperature development can probably be related to the onset of a La Niña episode towards the end of 2020 (Figure 28).

Neither of the Atlantic and Pacific longitudinal diagrams shows the extent to which the net changes displayed are caused by ocean dynamics operating east and west of the two profiles considered; they only display net changes along the longitudes chosen. For that reason, the diagrams should not be overinterpreted. The two longitudinal profiles, however, suggest an interesting contrast, with the Pacific Ocean mainly warming – especially north of Equator, and cooling in the south – while the opposite is seen in the Atlantic profile: cooling in the north and warming in the south.

(a) 2004–19

(b) 2019–20
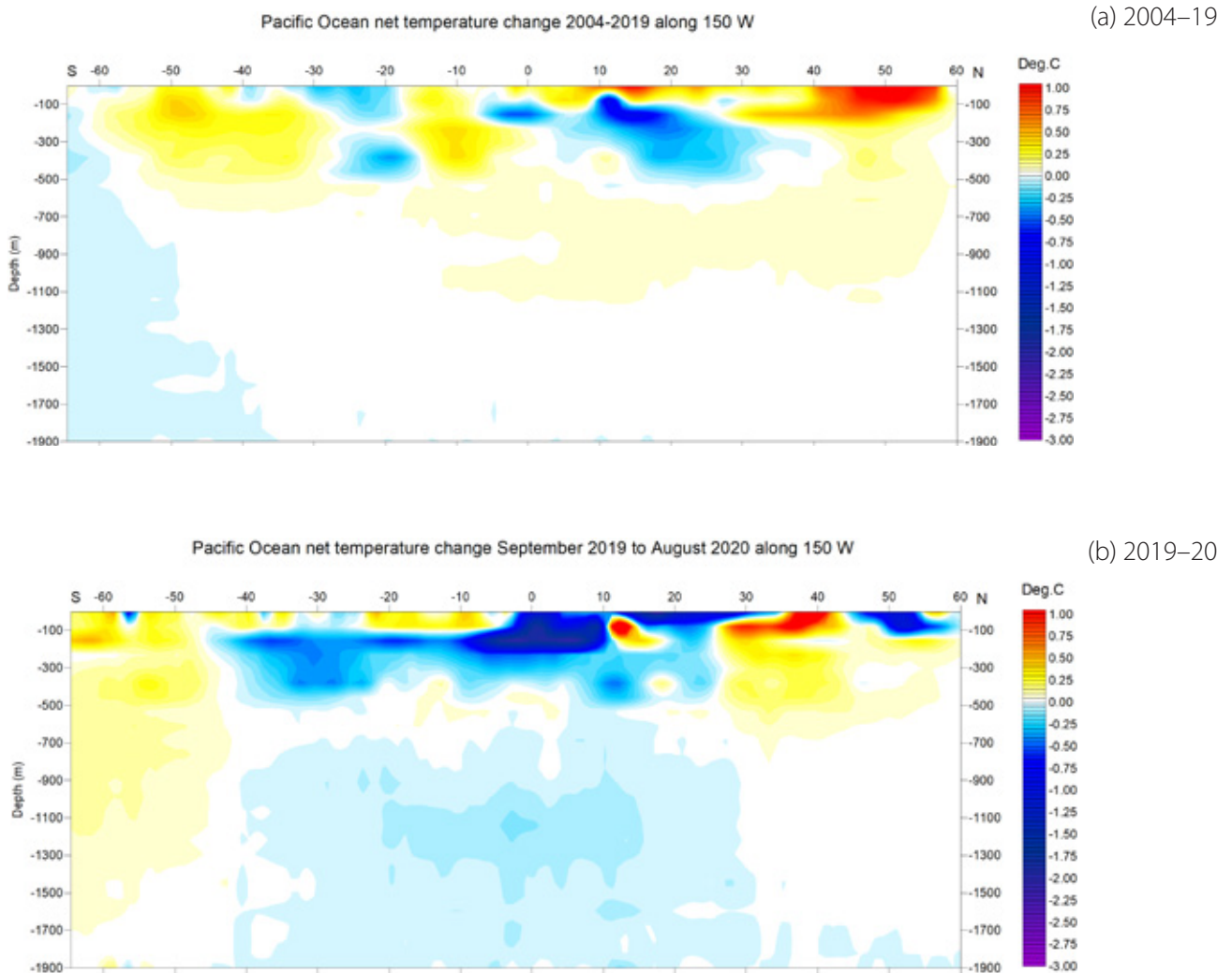
Figure 31: Temperature change along Pacific profile, 0–1900 m

(a) 2004–2019 and (b) Sept 19–Aug 20. See Figure 27 for geographical location of transect. Data source: Global Marine Argo Atlas.

19. Southern Oscillation Index

The Southern Oscillation Index (SOI) is calculated from the monthly or seasonal fluctuations in the air pressure difference between Tahiti and Darwin, Australia.

Sustained negative values of the SOI (Figure 32) often indicate El Niño episodes. Such negative values are usually accompanied by persistent warming of the central and eastern tropical Pacific Ocean, a decrease in the strength of the Pacific trade winds, and a reduction in rainfall over eastern and northern Australia.

Positive values of the SOI are usually associated with stronger Pacific trade winds and higher sea surface temperatures to the north of Australia, indicating La Niña episodes. Waters in the central and eastern tropical Pacific Ocean become cooler during this time. Eastern and northern Australia usually receive increased precipitation during such periods.

Figure 32: Annual SOI anomaly since 1866

The thin line represents annual values, while the thick line is the simple running 5-year average. Source: Climatic Research Unit, University of East Anglia.
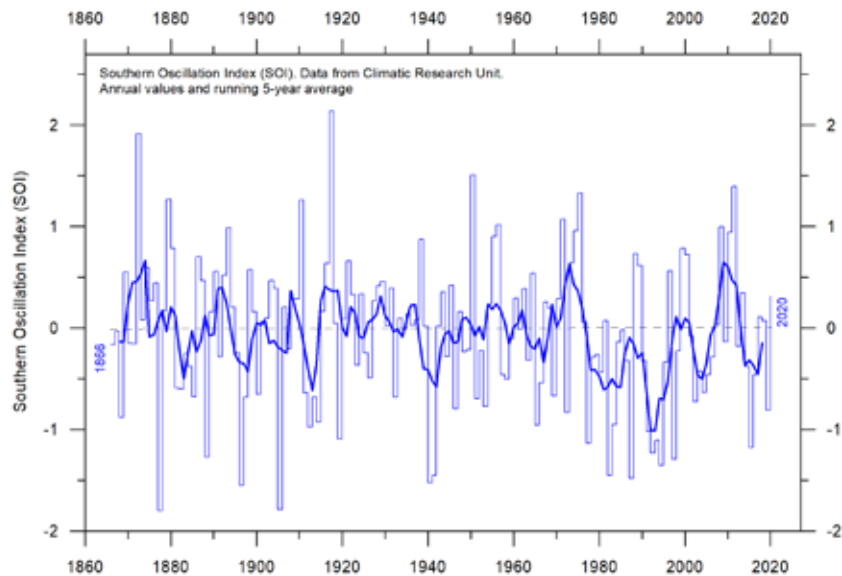
20. Pacific Decadal Oscillation

The Pacific Decadal Oscillation (PDO; Figure 33) is a long-lived El Niño-like pattern of Pacific climate variability, with data extending back to January 1854. The causes of the PDO are not currently known, but even in the absence of a theoretical understanding, PDO climate information improves season-to-season and year-to-year climate forecasts for North America because of its strong tendency for multi-season and multi-year persistence. The PDO also appears to be roughly in phase with global temperature changes. Thus, from a societal impact

Figure 33: Annual values of the Pacific Decadal Oscillation (PDO) according to the Physical Sciences Laboratory, NOOA.

The thin line shows the annual PDO values, and the thick line is the simple running 7-year average. Please note that the annual value of PDO is not yet updated beyond 2017. Source: PDO values from NOAA Physical Sciences Laboratory: ERSST V5 https://psl.noaa.gov/pdo/
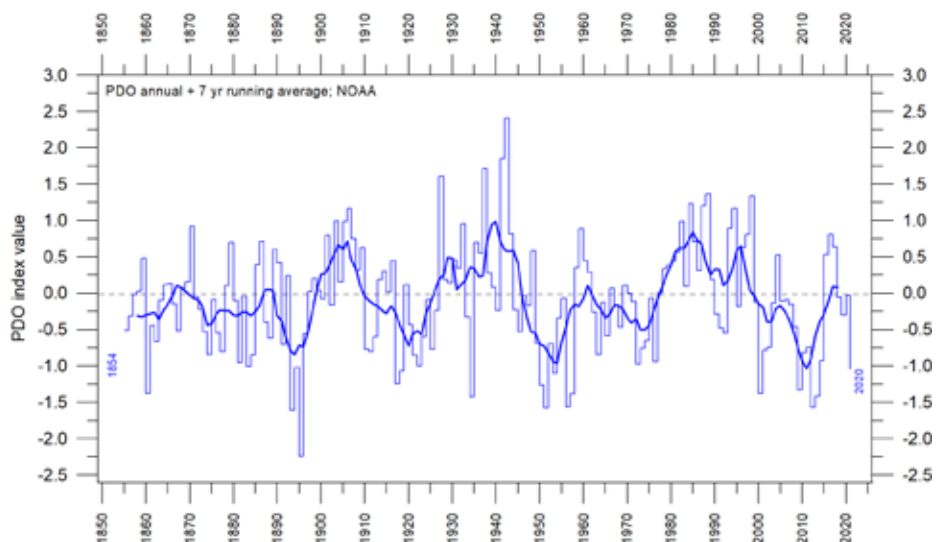
perspective, recognition of the PDO is important because it shows that 'normal' climate conditions can vary over time periods comparable to the length of a human lifetime.

The PDO nicely illustrates how global temperatures are tied to sea-surface temperatures in the Pacific Ocean, the largest ocean on Earth. When sea-surface temperatures are relatively low (negative-phase PDO), as from 1945 to 1977,

global air temperature decreases. When sea-surface temperatures are high (positive-phase PDO), as from 1977 to 1998, global surface air temperature increases (Figure 8, page 10).

A Fourier frequency analysis (not shown here) shows the PDO record (Figure 33) to be influenced by a 5.7-year cycle, and possibly also by a longer cycle of about 53 years.

21. Atlantic Multidecadal Oscillation

The Atlantic Multidecadal Oscillation (AMO; Figure 34) is a mode of variability occurring in the North Atlantic Ocean sea-surface temperature field. The AMO is essentially an index of North Atlantic sea-surface temperatures.

The AMO index appears to be correlated to air temperatures and rainfall over much of the Northern Hemisphere. The association appears to be high for North Eastern Brazil, African Sahel rainfall and North American and European summer climate. The AMO index also appears to be associated with changes in the frequency of North American droughts and is reflected in the frequency of severe Atlantic hurricanes.

As one example, the AMO index may be related to the past occurrence of major droughts

in the US Midwest and the Southwest. When the AMO is high, these droughts tend to be more frequent or prolonged, and vice-versa for low values of the AMO index. Two of the most severe droughts of the 20th century in US occurred during the peak AMO values between 1925 and 1965: the Dust Bowl of the 1930s and the 1950s' droughts. On the other hand, Florida and the Pacific Northwest tend to be the opposite; high AMO is here associated with relatively high precipitation.

A Fourier-analysis (not shown here) show the AMO record to be controlled by an about 67-year long cycle, and to a lesser degree by a 3.5-year cycle.
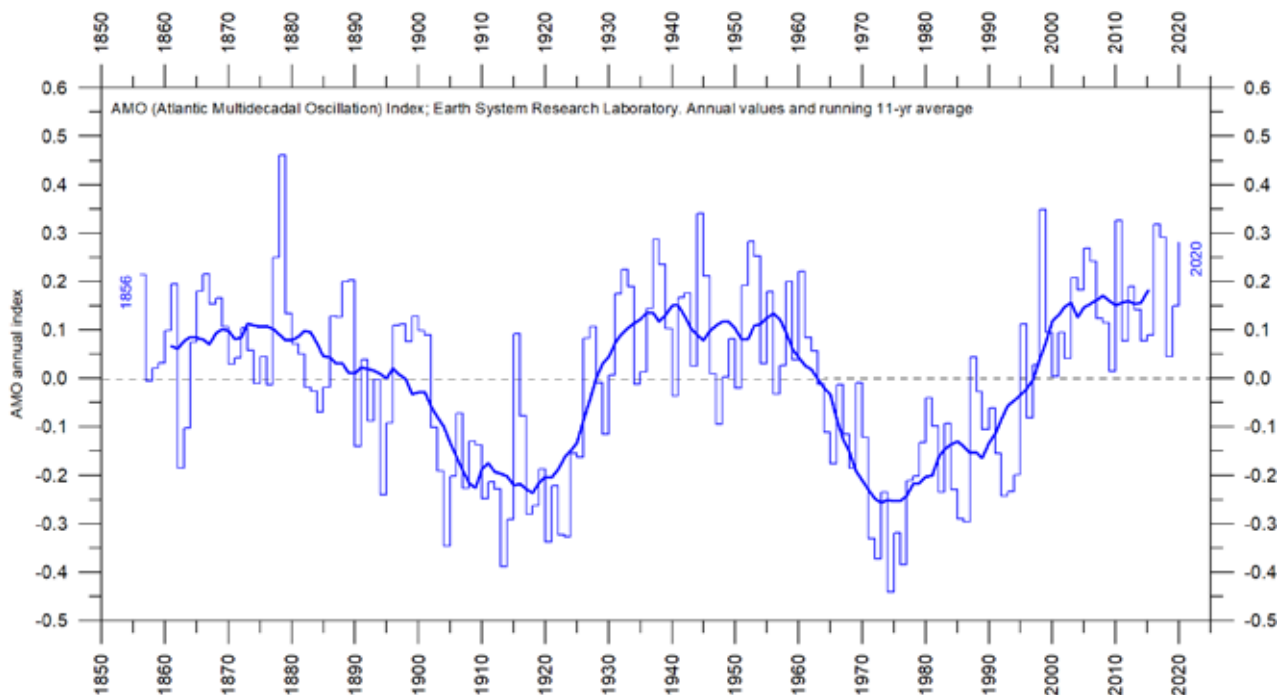
Figure 34: The Atlantic Multidecadal Oscillation

Annual Atlantic Multidecadal Oscillation (AMO) detrended and unsmoothed index values since 1856. The thin blue line shows annual values, and the thick line is the simple running 11-year average. Data source: Earth System Research Laboratory, NOAA, USA.

22. Sea level: general considerations

Global (or eustatic) sea-level change is measured relative to an idealised reference level called the geoid, which is a mathematical model of planet Earth's surface (Carter et al. 2014). Global sea level is a function of the volume of the ocean basins and the volume of water they contain. Changes in global sea level are caused by – but not limited to – four main mechanisms:

- Changes in local and regional air pressure and wind, and tidal changes introduced by the Moon.
- Changes in ocean basin volume by tec-

tonic (geological) forces.

- Changes in ocean water density caused by variations in currents, water temperature and salinity.
- Changes in the volume of water caused by changes in the mass balance of terrestrial glaciers.

In addition to these there are other mechanisms influencing sea level, such as storage of ground water, storage in lakes and rivers, evaporation, etc.

23. Sea level from satellite altimetry

Satellite altimetry is a relatively new and valuable type of measurement, providing unique insight into the detailed surface topography of the oceans, and any changes, with nearly global coverage. However, it is probably not a precise tool for estimating absolute changes in global

sea level due to assumptions made when interpreting the original satellite data.

One of the assumptions made when processing satellite altimetry data into sea level estimates (Figure 35) is the local and regional glacial isostatic adjustment (GIA). The GIA relates
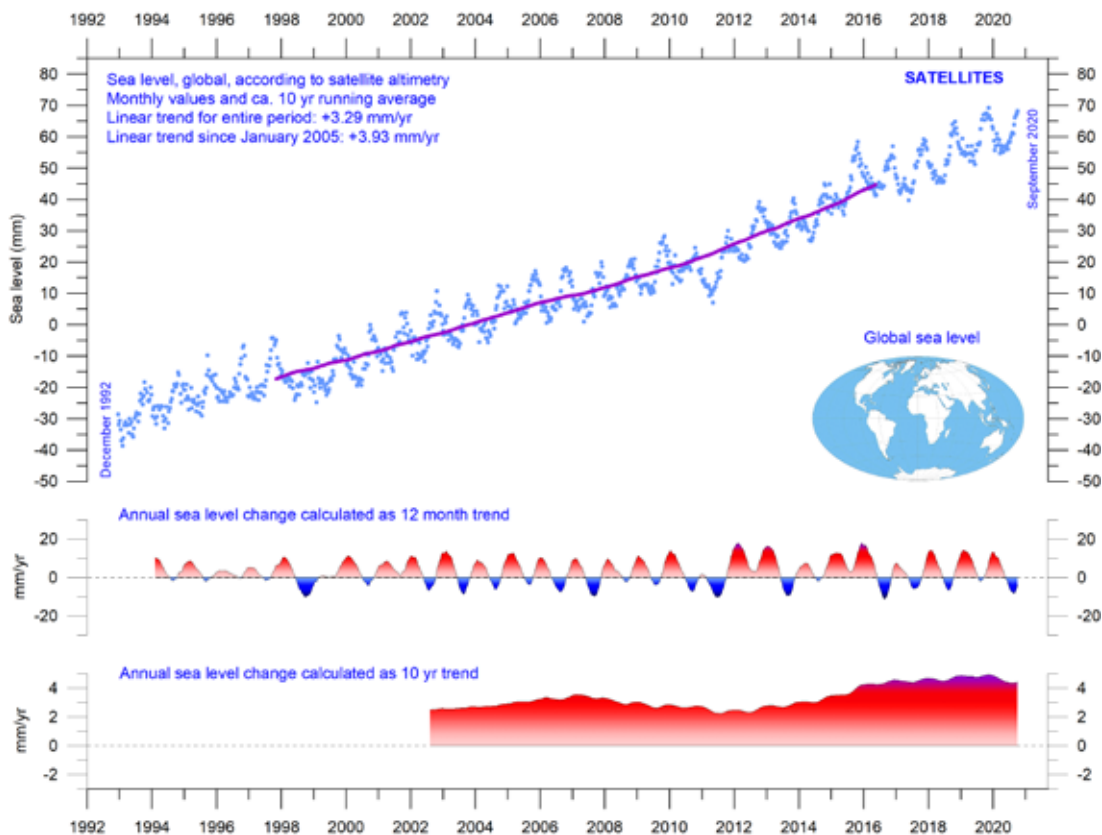
Figure 35: Global sea level change since December 1992

The two lower panels show the annual sea level change, calculated for 1- and 10-year time windows, respectively. These values are plotted at the end of the interval considered. Source: Colorado Center for Astrodynamics Research at University of Colorado at Boulder. The blue dots are the individual observations (with calculated GIA effect removed), and the purple line represents the running 121-month (ca. 10-year) average.

to large-scale, long-term mass transfer from the oceans to the land, in the form of rhythmic waxing and waning of the large Quaternary ice sheets in North America and North Europe. This enormous mass transfer causes cyclical changes in surface load, resulting in viscoelastic mantle flow and elastic effects in the upper crust. No single technique or observational network can give enough information on all aspects and consequences of the GIA, so the assumptions used for the interpretation of satellite altimetry data are difficult to verify. The value of the GIA introduced depends on the deglaciation and crust-mantle models that are used. Because of this (and additional factors), interpretations of modern global sea-level change based on satellite altimetry vary somewhat. In Figure 35, the global sea-level rise estimate is about 3.3 mm/year, with the estimated GIA effect removed.

24. Sea level from tide-gauges

Tide gauges record the net movement of the local ocean surface in relation to the land. Measurements of local relative sea-level change are vital information for coastal planning, in contrast to satellite altimetry.

In a precise context, the measured net movement of the local coastal sea-level is composed of two local components:

• the vertical change of the ocean surface, and

• the vertical change of the land surface.

For example, a tide gauge may record an apparent sea-level increase of 3 mm per year. If geodetic measurements show the land to be sinking by 2 mm per year, the real sea-level rise is only 1 mm per year (3 minus 2 mm). In a global sea-level change context, the value of 1 mm per year is the relevant one, but in a local coastal planning context, the 3 mm per year value obtained from the classical tide-gauge is the one
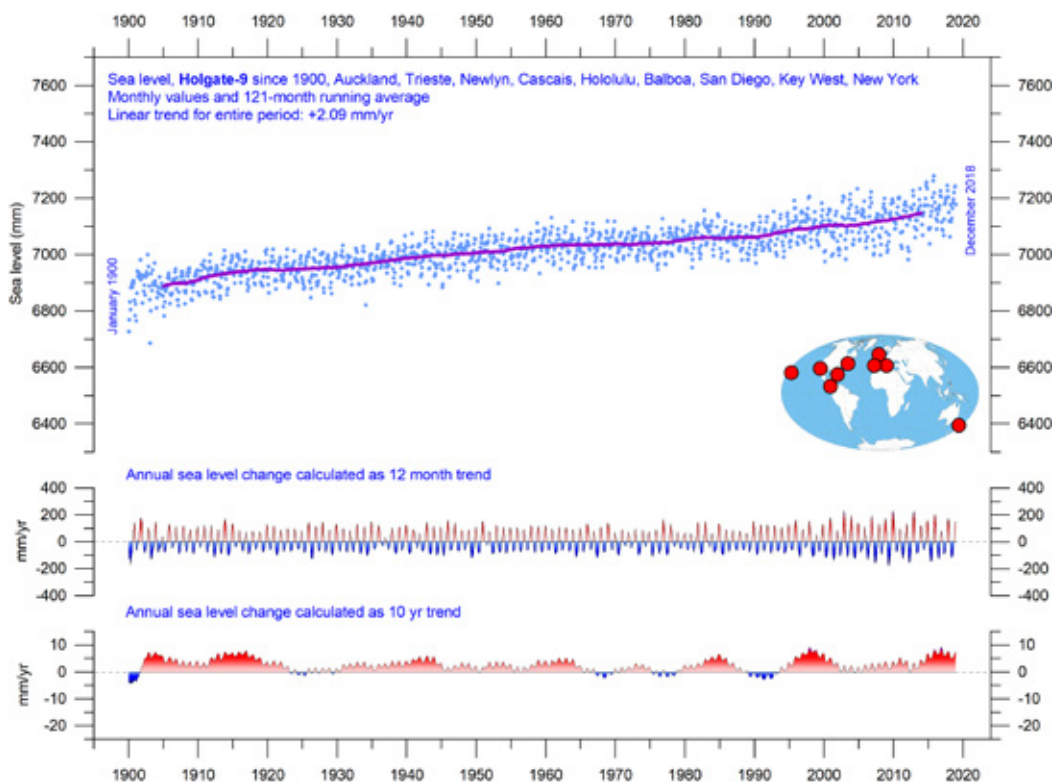
Figure 36: Holgate-9 monthly tide gauge data from PSMSL Data Explorer

The Holgate-9 are a series of tide gauges located in geologically stable sites. The two lower panels show the annual sea level change, calculated for 1- and 10-year time windows, respectively. These values are plotted at the end of the interval considered. Source: Colorado Center for Astrodynamics Research at University of Colorado at Boulder. The blue dots are the individual observations, and the purple line represents the running 121-month (ca. 10-year) average.

the local authorities should use.

To construct time series of sea-level measurements at each tide gauge, the monthly and annual means from gauge data supplied by national authorities must be reduced to a common datum. This reduction is performed by the Permanent Service for Mean Sea Level (PSMSL). The Revised Local Reference (RLR) datum at each station is defined to be approximately 7000 mm below mean sea level, with this arbitrary choice made many years ago to avoid negative numbers in the resulting RLR monthly and annual mean values.

Few places on Earth are completely stable, and most tide-gauges are located at sites exposed to tectonic uplift or sinking (the vertical change of the land surface). This widespread vertical instability has several causes, and affects the interpretation of data from the individual tide gauges. Much effort is therefore put into correcting for local tectonic movements.

Data from tide gauges located at tectoni-cally stable sites are therefore of particular interest for assessment of real short- and long-term sea-level change. One example is the long record from Korsør, Denmark (Figure 37), which indicates a stable sea-level rise of about 0.83 mm per year, with no indication of recent acceleration.

Data from tide gauges all over the world suggest an average global sea-level rise of 1–2 mm/year, while the satellite-derived record (Figure 35) suggests a rise of about 3.3 mm/year, or more. The difference between the two datasets (a ratio of about 1:2) is remarkable but has no generally accepted explanation. It is, however, known that satellite observations face complications in coastal areas. Vignudelli et al. (2019) provide an updated overview of the current limitations of classical satellite altimetry in coastal regions. Goklany (2021) provides several additional reflections on ongoing sea-level change.
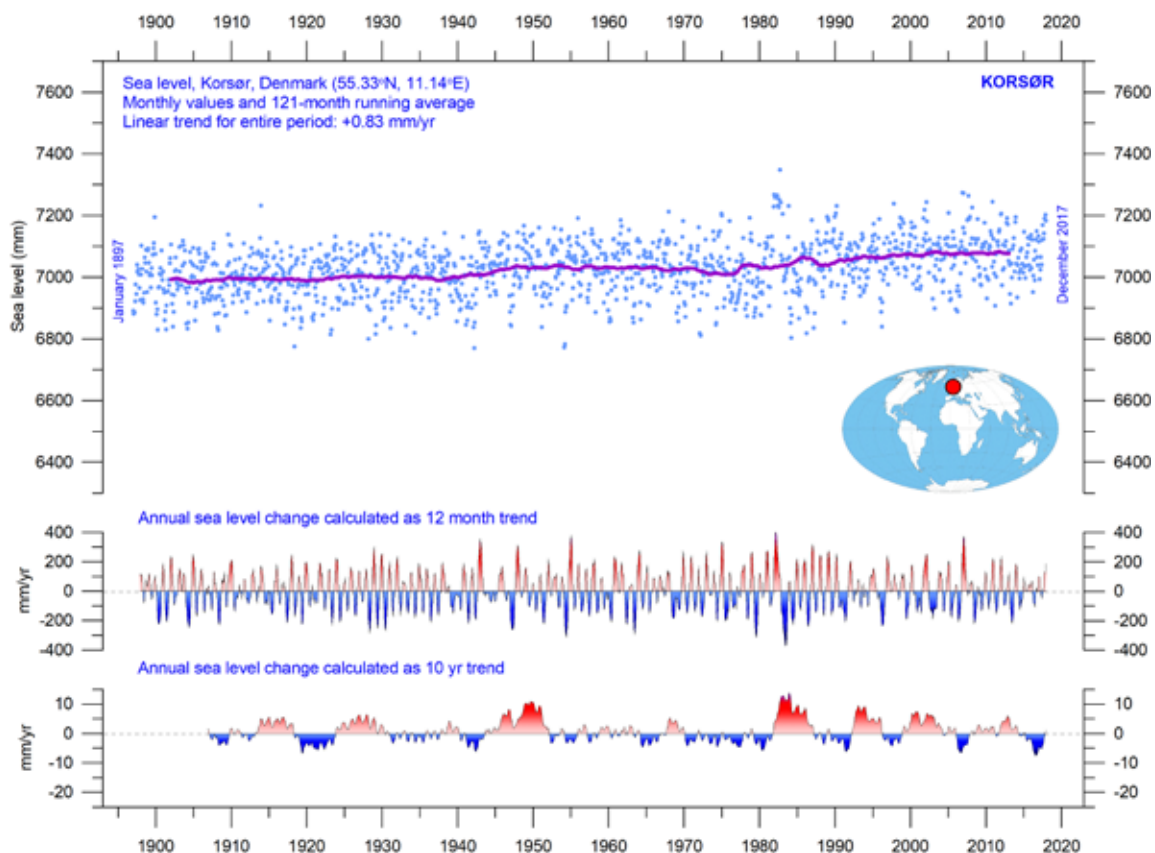
Figure 37: Korsør (Denmark) monthly tide gauge data

From PSMSL Data Explorer. The blue dots are the individual monthly observations, and the purple line represents the running 121-month (ca. 10-year) average. The two lower panels show the annual sea level change, calculated for 1- and 10-year time windows, respectively. These values are plotted at the end of the interval considered.

25. Global, Arctic and Antarctic sea-ice extent

The two 12-month average sea-ice extent graphs for 1979–2020 shown in Figure 38 reveal a contrasting trend between the two poles. Sea ice in the Northern Hemisphere has been decreasing, but there was a simultaneous increase of Southern Hemisphere sea-ice extent, lasting until 2016.

The Antarctic sea-ice extent decreased extremely rapidly during the Southern Hemisphere spring of 2016, much faster than in any previous spring during the satellite era (since 1979). A strong sea-ice retreat occurred in all sectors of the Antarctic, but was greatest in the Weddell and Ross Seas. In these sectors, strong
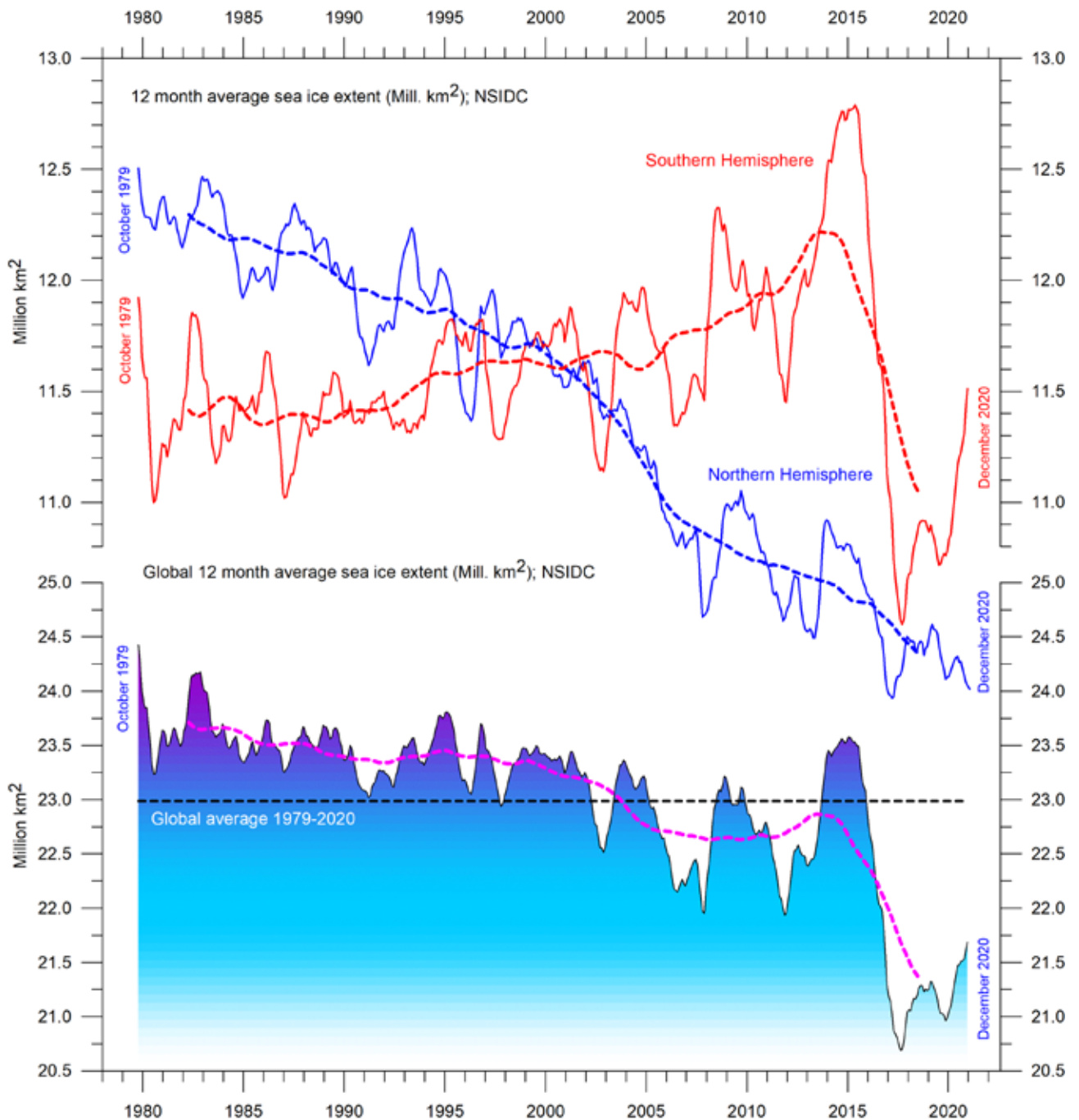
Figure 38: Global and hemispheric sea ice extent since 1979

12-month running means. The October 1979 value represents the monthly average of November 1978–October 1979, the November 1979 value represents the average of December 1978–November 1979, etc. The stippled lines represent a 61-month (ca. 5 years) average. The last month included in the 12-month calculations is shown to the right in the diagram. Data source: National Snow and Ice Data Center (NSIDC).

34

northerly (warm) surface winds pushed the sea ice back towards the Antarctic continent. The background for the special wind conditions in 2016 has been discussed by various authors (e.g. Turner et al. 2017 and Phys.org 2019) and appears to be a phenomenon related to natural climate variability. The satellite sea-ice record is still short, and does not fully represent natural variations playing out over more than a decade or two.

What can be identified from the still-short record is nevertheless instructive. The two 12-month average graphs in Figure 38 are visually characterised by recurring variations, superimposed on the overall trends. For the Arctic, this shorter variation is strongly influenced by a 5.3-year cycle, while for the Antarctic, a periodic variation of about 4.5 years is important. Both these variations reached their minima simultaneously in 2016, which at least partly explains the simultaneous minimum in global sea-ice extent.

In coming years, these variations may again induce increases in sea-ice extent at both poles, with a resultant increase in the 12-month global average. In fact, this may already have begun in the Antarctic (Figure 38). And in the Arctic, the average ice thickness also shows signs of increasing (Figure 39). However, in coming years, the minima and maxima for these variations will not be synchronous because of their different periods, and global minima (or maxima) may therefore be less pronounced than in 2016.

The diagrams in Figure 39 illustrate the overall extent and thickness of the Arctic sea ice from the end of 2019 to the end of 2020, as published by the Danish Meteorological Institute. The most conspicuous change over this period was an overall increase in ice thickness in the central part of the Arctic Ocean. In addition, relatively thicker sea ice has established itself north of Canada and Greenland, compared to the situation at the end of 2019.
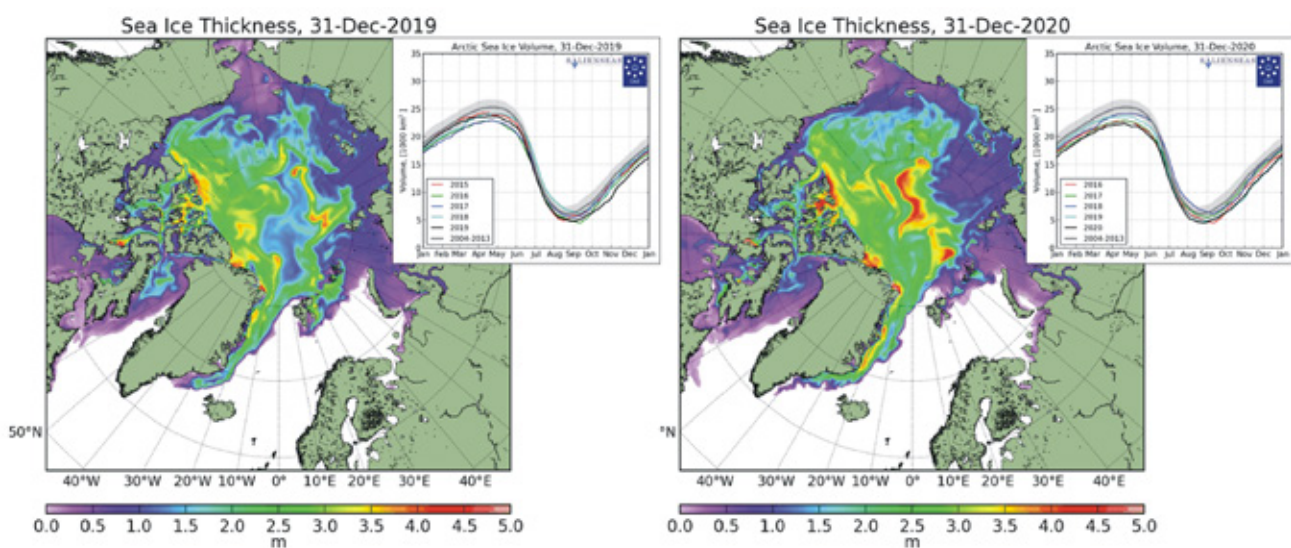
Figure 39: Arctic sea ice 2019 versus 2020

Arctic sea-ice extent and thickness 31 December 2019 (left) and 2020 (right) and the seasonal cycles of the calculated total arctic sea ice volume, according to the Danish Meteorological Institute (DMI). The mean sea ice volume and standard deviation for the period 2004–2013 are shown by grey shading in the insert diagrams.

26.   Northern Hemisphere snow cover extent

Variations in the global snow cover extent are mainly due to changes playing out in the Northern Hemisphere (Figure 40), where all the major land areas are located. The Southern Hemisphere snow cover extent is essentially determined by the Antarctic Ice Sheet, and is therefore relatively stable.

The Northern Hemisphere snow cover extent is subject to large local and regional variations from year to year. However, the overall tendency (since 1972) is towards stable Northern Hemisphere snow conditions, as illustrated in Figure 41.

During the Northern Hemisphere sum-mer, the snow cover usually shrinks to about 2,400,000 km^2 (principally controlled by the size of the Greenland Ice Sheet), and during the Northern Hemisphere winter the snow-covered area increases to about 50,000,000 km^2, representing no less than 33% of planet Earth's total land area.

Considering seasonal changes (Figure 42), Northern Hemisphere snow cover extent during autumn has been slightly increasing, the mid-winter extent is basically stable, and the spring extent has been slightly decreasing. In 2020, the Northern Hemisphere snow cover extent was slightly below the 1972–2020 average.
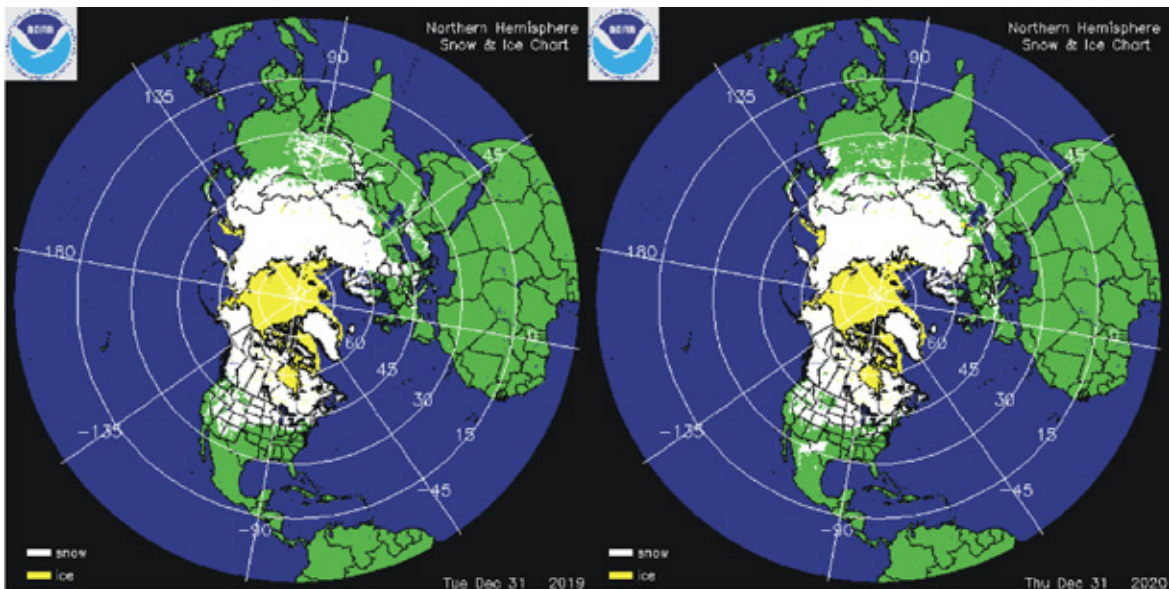
Figure 40: Northern hemisphere snow and sea ice

Snow cover (white) and sea ice (yellow) 31 December 2019 (left) and 2020 (right). Map source: National Ice Center (NIC).
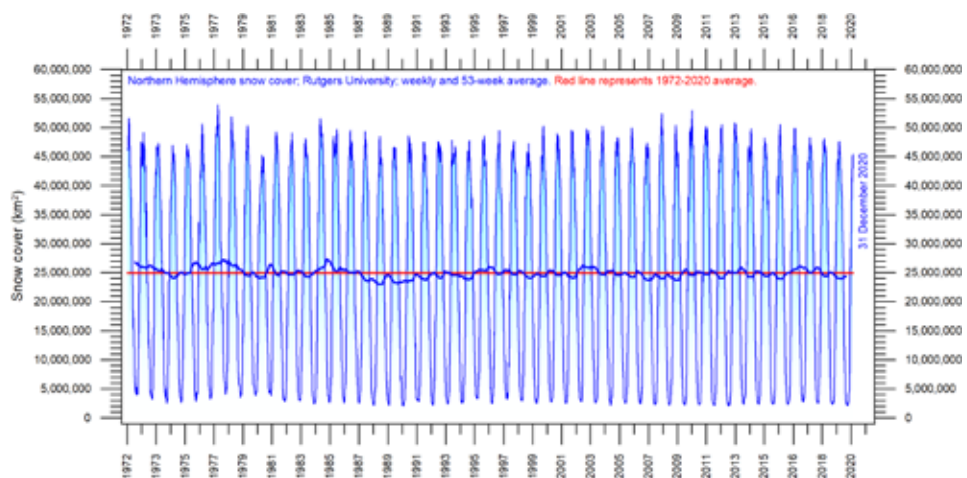
Figure 41: Northern hemisphere weekly snow cover since 1972

Source: Rutgers University Global Snow Laboratory. The thin blue line is the weekly data, and the thick blue line is the running 53-week average (approximately 1 year). The horizontal red line is the 1972–2020 average.
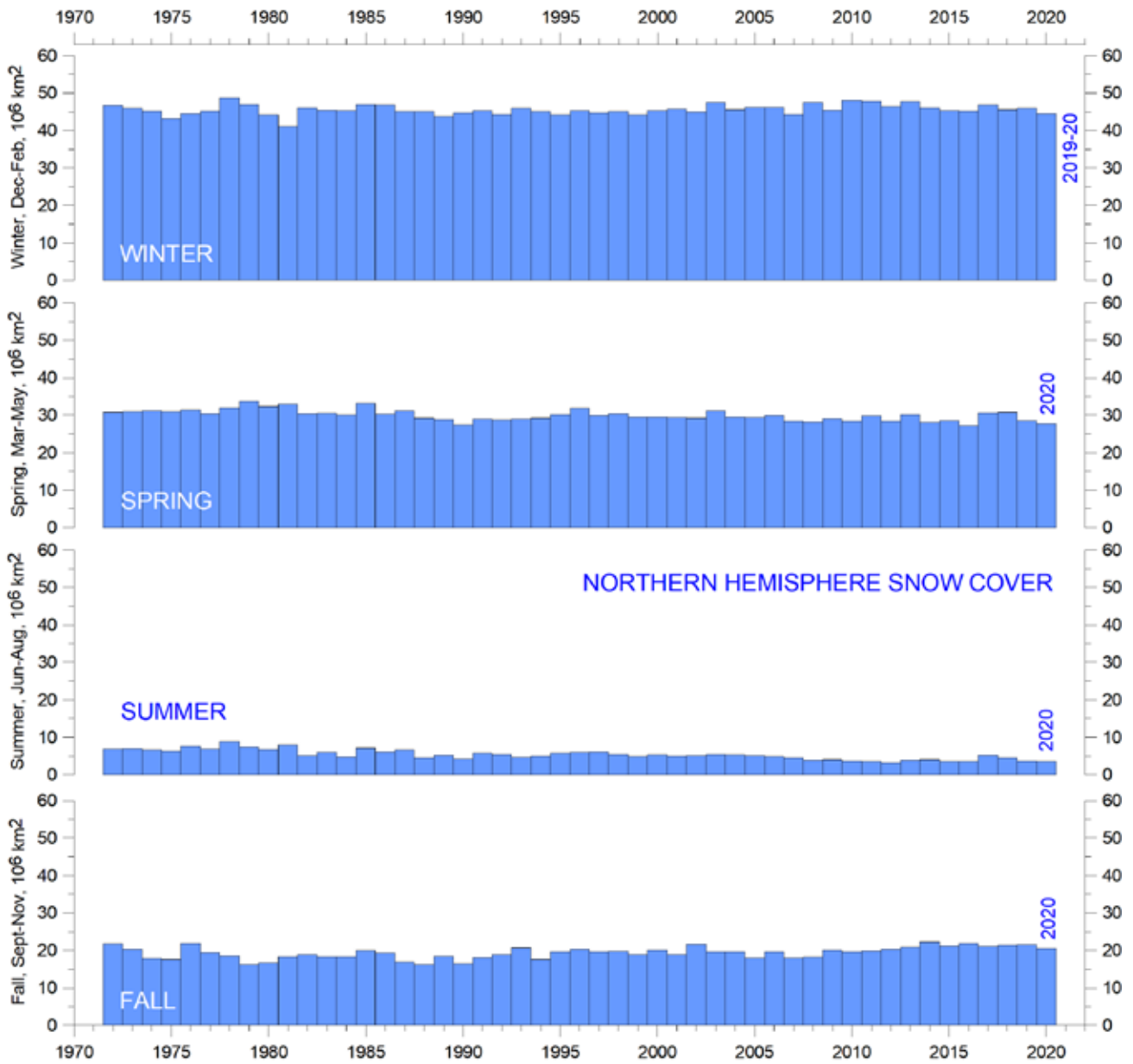
Figure 42: Northern Hemisphere seasonal snow cover since 1972

Data source: Rutgers University Global Snow Laboratory.

27.   Tropical storm and hurricane accumulated cyclone energy

Accumulated cyclone energy (ACE) is a measure used by the US National Oceanic and Atmospheric Administration to express the activity of individual tropical cyclones and entire tropical cyclone seasons. ACE is calculated as the square of the wind speed every 6 hours and is then scaled by a factor of 10,000 for usability. It has a unit of 10^4 knots[2]. The ACE of a season is the sum of the ACE for each storm and considers the number, strength, and duration of all the tropical storms in the season.

The damage potential of a hurricane is proportional to the square or cube of the maximum wind speed, and thus ACE is therefore not only a measure of tropical cyclone activity, but also a measure of the damage potential of an individual cyclone or a season. Existing records (Figure 43) do not suggest any abnormal cyclone activity in recent years.

The global ACE data since 1970 display a variable pattern over time (Figure 43), but without any clear trend, as are the diagrams for the Northern and Southern Hemispheres. A Fourier analysis (not shown here) reveals a significant period of about 3.6 years in the ACE data, and furthermore suggests the existence of a 11.5-year period, but the data series is still too short to draw conclusions.
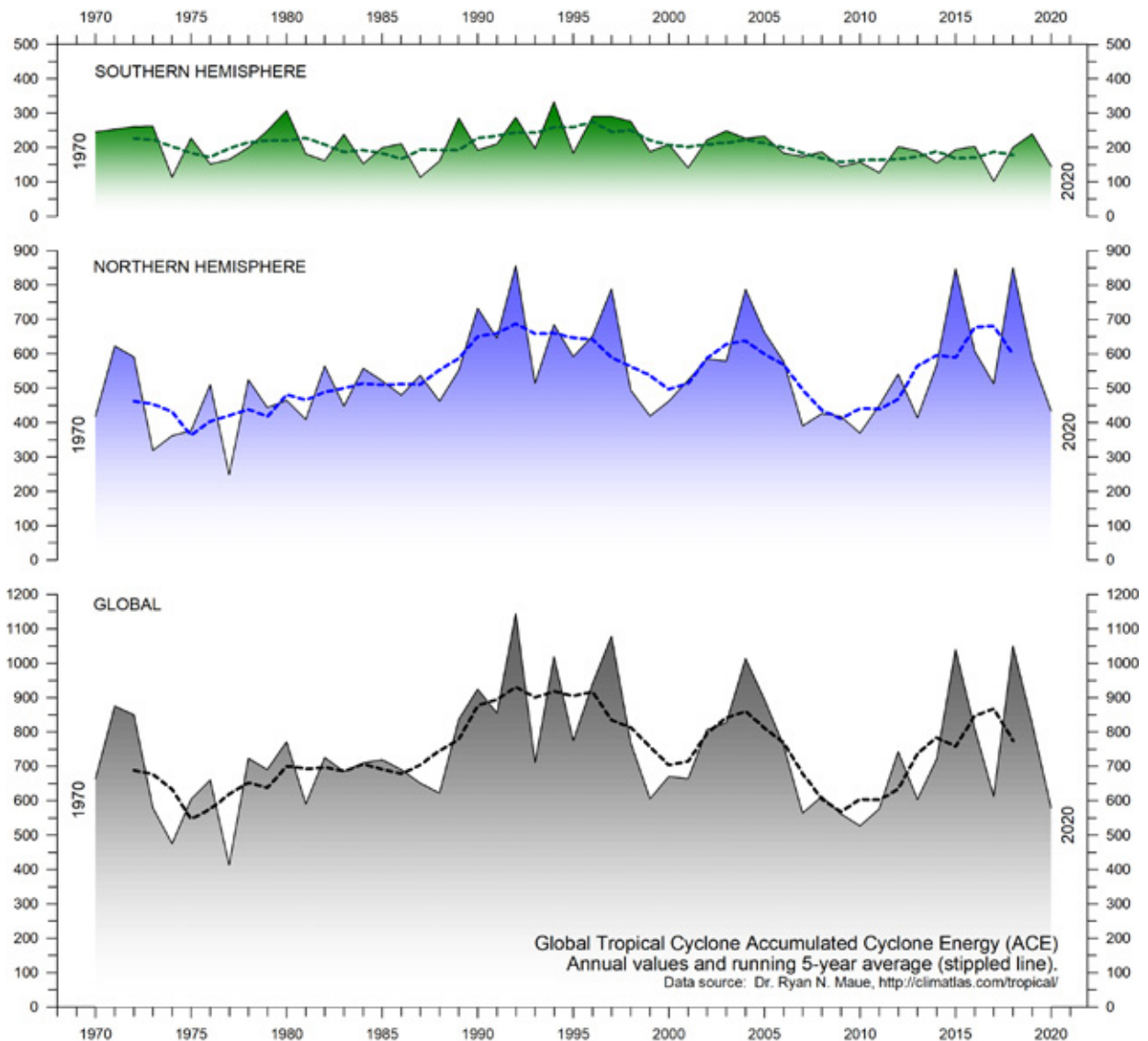
Figure 43: Annual global ACE

Source: Ryan Maue.

The period 1989–1998 was characterised by high values, and other peaks were seen 2004, 2015 and 2018, while the periods 1973–1988, 1999–2003 and 2006–2014 were characterised by low values. The peaks in 1997/98 and 2016 coincided with strong El Niño events in the Pacific Ocean (Figure 22). The ACE data and ongoing cyclone dynamics are detailed in Maue (2011). The Northern Hemisphere ACE values (central panel in Figure 43) dominate the global signal (lower panel in Figure 43) and therefore show similar peaks and troughs as displayed by the global data, without any clear trend for the entire observational period. The Northern Hemisphere main cyclone season is June–November. The Southern Hemisphere ACE values (lower panel in Figure 39) are generally lower than for the Northern Hemisphere, and the main cyclone season is December–April.

The Atlantic Oceanographic and Meteorological Laboratory ACE data series goes back to 1850. A Fourier analysis for the Atlantic Basin (Figure 44) reveals the ACE series to be strongly influenced by a periodic variation of about 60 years' duration. At present, since 2002, the Atlantic ACE series has an overall declining trend, but with large interannual variations. The North Atlantic hurricane season often shows above-average activity when La Niña conditions are present in Pacific during late summer (August–October), as was the case in 2017 (Johnstone and Curry, 2017).

Goklany (2021) presents many additional observations and reflections on recent storm and hurricane activity.
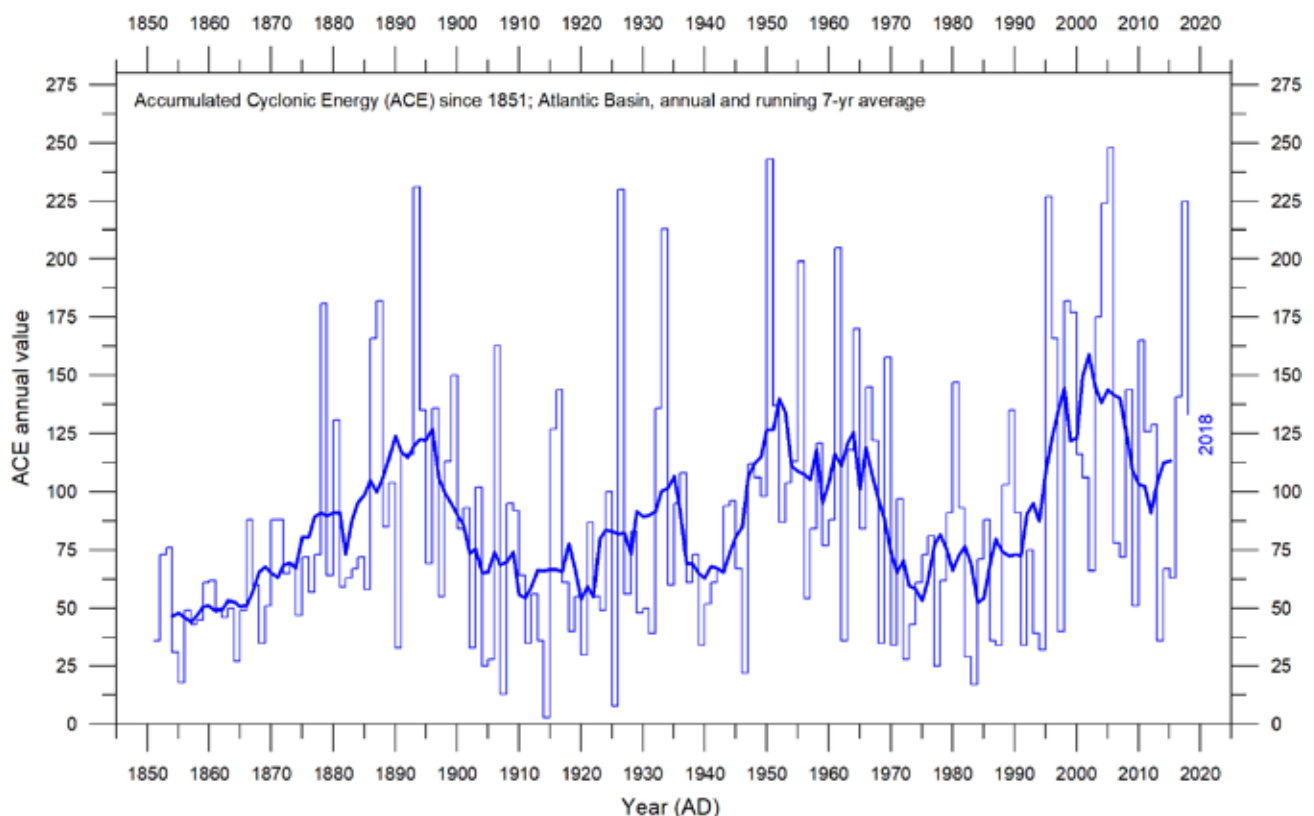
Figure 44: Atlantic basin ACE since 1851

Thin lines show annual ACE values, and the thick line shows the running 7-year average. Data source: Atlantic Oceanographic and Meteorological Laboratory (AOML), Hurricane Research Division. Please note that these data are not yet updated beyond 2018.

28. Other storm and wind observations

Figure 45 shows the number of hurricane landfalls in the continental United States. There are considerable variations from year to year, but it is not possible to detect any clear trend. A Fourier analysis (not shown here) reveals this annual data series to be characterised by two statistically significant periods, of about 3.2 and 4.9 years, respectively.

Insight into changes of prevailing wind conditions may also be obtained from the inspection of observations carried out at coastal meteorological stations, situated at particularly wind-exposed places. One example, from northwest Europe, is Lista Lighthouse in Norway. The lighthouse sits on an exposed cape at the extreme southwestern edge of the mainland of the country, well suited to register wind conditions in the adjoining North Sea and the European sector of the North Atlantic. Lista Lighthouse has a monthly wind record going back to January 1931, as displayed in Figure 46. At this location, the peak wind strengths were recorded shortly after World War II and have since declined somewhat, to some degree reflecting the overall development displayed by the number of Continental United States Hurricane landfalls (Figure 45); that is, on the opposite shore of the North Atlantic.
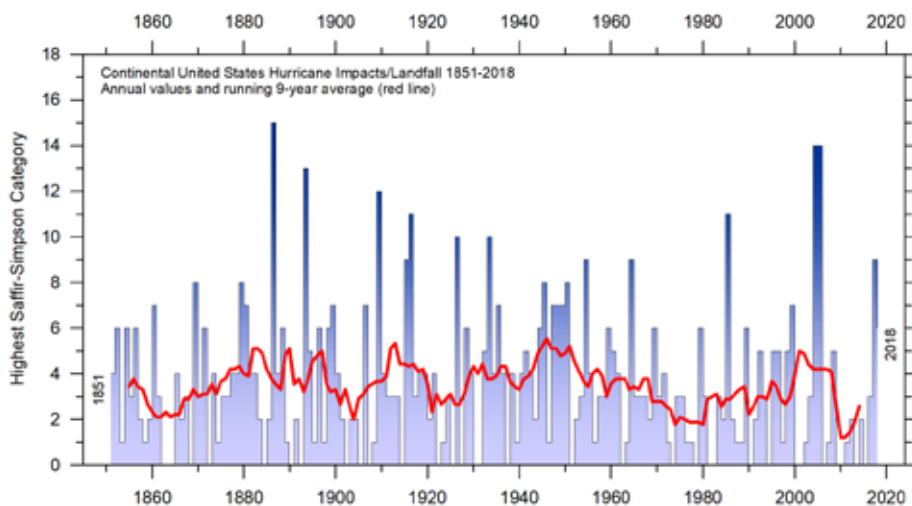
Figure 45: Hurricane landfalls in the continental United States 1851–2018

The highest Saffir-Simpson Hurricane Scale impact in the United States is based upon estimated maximum sustained surface winds produced at the coast. Data source: Hurricane Research Division, NOAA. Please note that this data series is not yet updated beyond 2018.
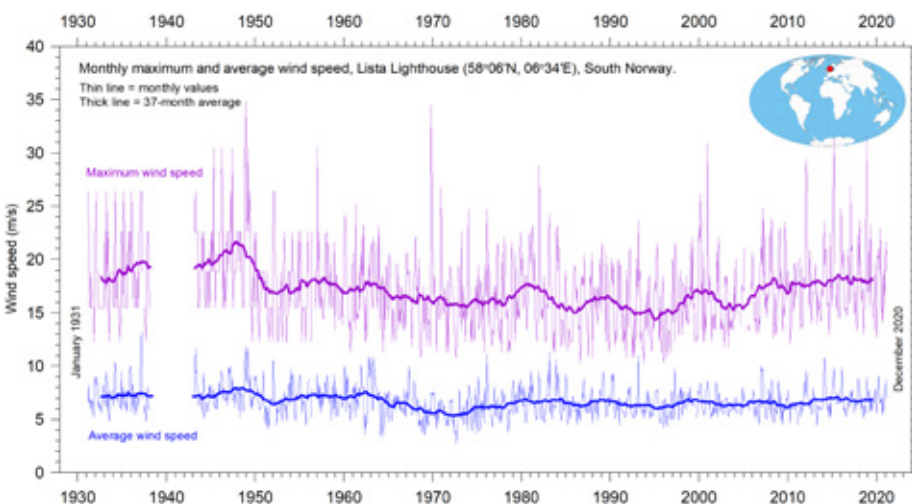
Figure 46: Monthly maximum and average wind speed since January 1931 measured at Lista Lighthouse, South Norway

Lista Lighthouse is situated on an exposed cape located at the extreme southwestern edge of mainland Norway, in a position to register wind conditions in the adjoining North Sea and the European sector of the North Atlantic. Data source: SeKlima. Not yet updated beyond 2018.

29. References

Carter R.M. et al. (2014). *Commentary and Analysis on the Whitehead & Associates 2014 NSW Sea-Level Report*. Policy Brief, NIPCC, 24 September 2014. http://climatechangereconsidered.org/wp-content/uploads/2014/09/NIPCC-Report-on-NSW-Coastal-SL-9z-corrected.pdf.

Chylek, P. et al. (2010). Twentieth century bipolar seesaw of the Arctic and Antarctic surface air temperatures. *Geophysical Research Letters*, 37, L08703, doi:10.1029/2010GL042793.

Goklany, I.M. (2021). *Impacts of Climate Change Perception and Reality*. The Global Warming Policy Foundation, report 46, 44pp. https://www.thegwpf.org/content/uploads/2021/02/Goklany-EmpiricalTrends.pdf.

Holgate, S.J. (2007). On the decadal rates of sea level change during the twentieth century. *Geophysical Research Letters*; 34: L01602, doi:10.1029/2006GL028492.

Jaworowski, Z. et al. (1992). Do glaciers tell a true atmospheric CO_2 story? *The Science of the Total Environment*; 114: 227–284. https://www.researchgate.net/publication/223504148_Do_glaciers_tell_a_true_atmospheric_CO2_story.

Johnstone, J. and Curry, J. (2017). *Causes and Predictability of the Exceptionally Active 2017 Atlantic Hurricane Season*. Climate Forecast Applications Network. https://curryja.files.wordpress.com/2017/11/hurricane_review_2017-final.pdf.

Lindzen, R.S. and Christy, J.R. (2020). *The Global Mean Temperature Record. How it works and why it is misleading*. CO_2 Coalition. http://co2coalition.org/publications/the-global-mean-temperature-anomaly-record/.

Maue, R.L. (2011). Recent historically low global tropical cyclone activity. *Geophysical Research Letters*; 38: L14803, doi:10.1029/2011GL047711.

Roemmich, D. and Gilson J. (2009). The 2004–2008 mean and annual cycle of temperature, salinity, and steric height in the global ocean from the Argo Program. *Progress in Oceanography*; 82: 81–100.

Turner J. et al. (2017). Unprecedented springtime retreat of Antarctic sea ice in 2016. *Geophysical Research Letters*; 44(13): 6868–6875. https://doi.org/10.1002/2017GL073656.

Vignudelli et al. (2019). Satellite altimetry measurements of sea level in the coastal zone. *Surveys in Geophysics, Vol.* 40, 1319–1349. https://link.springer.com/article/10.1007/s10712-019-09569-1.

30. Links to data sources

All sources accessed January–March 2021.

AMO, Earth System Research Laboratory, NOAA, USA: https://www.esrl.noaa.gov/psd/data/timeseries/AMO/.

Atlantic Oceanographic and Meteorological Laboratory, Hurricane Research Division: http://www.aoml.noaa.gov/hrd/tcfaq/E11.html.

Colorado Center for Astrodynamics Research: http://sealevel.colorado.edu/.

Danish Meteorological Institute (DMI): http://ocean.dmi.dk/arctic/icethickness/thk.uk.php.

Earth System Research Laboratory (ESRL): https://www.esrl.noaa.gov/psd/map/clim/olr.shtml.

GISS temperature data: https://data.giss.nasa.gov/gistemp/.

Global Marine Argo Atlas: http://www.argo.ucsd.edu/Marine_Atlas.html.

Goddard Institute for Space Studies (GISS): https://www.giss.nasa.gov/.

HadCRUT temperature data: http://hadobs.metoffice.com/.

Hurricane Research Division, NOAA: http://www.aoml.noaa.gov/hrd/tcfaq/E23.html.

National Ice Center (NIC). http://www.natice.noaa.gov/pub/ims/ims_gif/DATA/cursnow.gif.

National Snow and Ice Data Center (NSIDC): http://nsidc.org/data/seaice_index/index.html.

NCDC temperature data: https://www.ncdc.noaa.gov/monitoring-references/faq/.

Ocean temperatures from Argo floats: http://www.argo.ucsd.edu/.

Oceanic Niño Index (ONI): http://www.cpc.ncep.noaa.gov/products/analysis_monitoring/ensos-tuff/ensoyears.shtml.

Outgoing long-wave radiation (OLR): https://www.esrl.noaa.gov/psd/map/clim/olr.shtml.

PDO, NOAA Physical Sciences Laboratory: https://psl.noaa.gov/pdo/.

Permanent Service for Mean Sea Level: http://www.psmsl.org/.

Phys.org 2019: https://phys.org/news/2019-01-antarctica-sea-ice-climate.html.

Plymouth State Weather Center: http://vortex.plymouth.edu/sfc/sst/.

PSMSL Data Explorer: http://www.psmsl.org/data/obtaining/map.html.

Rutgers University Global Snow Laboratory: http://climate.rutgers.edu/snowcover/index.php.

RSS temperature data: http://www.remss.com/measurements/upper-air-temperature.

Sea level from satellites: https://sealevel.colorado.edu/data/2020rel1-global-mean-sea-level-sea-sonal-signals-retained.

Sea level from tide gauges: http://www.psmsl.org/data/obtaining/map.html.

Sea-ice extent Danish Meteorological Institute (DMI): http://ocean.dmi.dk/arctic/icethickness/thk.uk.php.

SeKlima: https://seklima.met.no/observations/.

Southern Oscillation Index (SOI): http://crudata.uea.ac.uk/cru/data/soi/.

Maue ACE data: climatlas.com/tropical/.

UAH temperature data: http://www.nsstc.uah.edu/data/msu/v6.0/tlt/uahncdc_lt_6.0.txt.

Review process

GWPF publishes papers in a number of different formats, with a different review process pertaining to each.

- Our flagship long-form GWPF Reports, are all reviewed by our Academic Advisory Panel.
- GWPF Briefings and Notes are shorter documents and are reviewed internally and/or externally as required.

Part of the function of the review process is to ensure that any materials published by the GWPF are of a proper academic standard, and will serve the GWPF's educational purpose. As a charity, we recognise that educational material should provide any reader the opportunity to understand, and explore different perspectives on a subject.

This means that, for most publications, we also invite an external review from a party who we would expect to take a different view to the publication's author. We offer to publish any substantive comments alongside the main paper, provided we are satisfied they will enhance the educational experience of the reader. In this way, we hope to encourage open and active debate on the important areas in which we work.

This enhanced review process for GWPF papers is intended to take the content and analysis beyond a typical review for an academic journal:

- More potential reviewers can be involved
- The number of substantive comments will typically exceeds journal peer review, and
- The identity of the author is known to the potential reviewers.

As an organisation whose publications are sometimes the subject of assertive or careless criticism, this review process is intended to enhance the educational experience for all readers, allowing points to be made and considered in context and observing the standards required for an informed and informative debate. We therefore expect all parties involved to treat the reviews with the utmost seriousness.

Final responsibility for publication rests with the Chairman of the Trustees and the GWPF Director. But in every case, the views expressed are those of the author. GWPF has never had any corporate position beyond that dictated by its educational objectives.

About the Global Warming Policy Foundation

The Global Warming Policy Foundation is an all-party and non-party think tank and a registered educational charity which, while openminded on the contested science of global warming, is deeply concerned about the costs and other implications of many of the policies currently being advocated.

Our main focus is to analyse global warming policies and their economic and other implications. Our aim is to provide the most robust and reliable economic analysis and advice. Above all we seek to inform the media, politicians and the public, in a newsworthy way, on the subject in general and on the misinformation to which they are all too frequently being subjected at the present time.

The key to the success of the GWPF is the trust and credibility that we have earned in the eyes of a growing number of policy makers, journalists and the interested public. The GWPF is funded overwhelmingly by voluntary donations from a number of private individuals and charitable trusts. In order to make clear its complete independence, it does not accept gifts from either energy companies or anyone with a significant interest in an energy company. **Views expressed in the publications of the Global Warming Policy Foundation are those of the authors, not those of the GWPF, its trustees, its Academic Advisory Council members or its director.**

RECENT GWPF REPORTS

GWPF